

# EEG-FM-Bench: A Comprehensive Benchmark for the Systematic Evaluation and Diagnostic Analyses of EEG Foundation Models

Wei Xiong<sup>1</sup> Jiangtong Li<sup>1</sup> Jie Li<sup>2,1</sup> Kun Zhu<sup>1</sup> Changjun Jiang<sup>1</sup>

## Abstract

Electroencephalography foundation models (EEG-FMs) have advanced brain signal analysis, but the lack of standardized evaluation benchmarks impedes model comparison and scientific progress. Current evaluations rely on inconsistent protocols that render cross-model comparisons unreliable, while a lack of diagnostic analyses obscures the internal mechanisms driving transfer efficiency and scaling behaviors. To address this, we introduce **EEG-FM-Bench**, a unified system for the standardized evaluation of EEG-FMs. The benchmark integrates 14 datasets across 10 paradigms and incorporates diverse experimental settings, including multiple fine-tuning strategies, task organizations, and classifier configurations, supported by tools for gradient and representation analysis. Our experiments and analysis reveal several critical insights: (1) multi-task learning acts as a critical regularizer to mitigate overfitting in data-scarce EEG contexts; (2) pre-training efficiency is currently limited by gradient conflicts between reconstruction objectives and downstream tasks; (3) model scaling deviates from typical laws, as compact architectures with domain-specific inductive biases consistently outperform significantly larger models. This benchmark enables fair comparison and reproducible analysis, shifting the field from fragmented results to interpretable advances. Code is available at <https://github.com/xw1216/EEG-FM-Bench>.

<sup>1</sup>School of Computer Science and Technology, Tongji University, Shanghai, China <sup>2</sup>Translational Research Center, Shanghai Yangzhi Rehabilitation Hospital (Shanghai Sunshine Rehabilitation Center), China. Correspondence to: Wei Xiong <xw1216@tongji.edu.cn>.

Preprint. February 16, 2026.

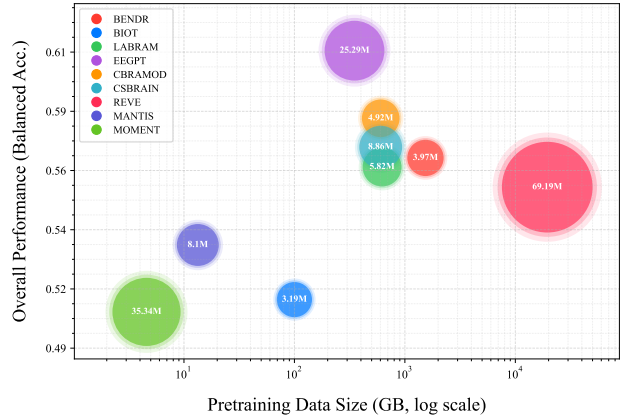


Figure 1. **Scaling analysis: Performance vs. Data and Model Size.** We plot the overall balanced accuracy against pre-training data size. Bubble size represents the model parameter count.

## 1. Introduction

Due to the high temporal resolution, non-invasiveness, and cost-effectiveness, EEG is widely used in neuroscience and clinical scenarios, ranging from cognition to pathology (Ramantani et al., 2016). Following the success of large-scale pre-training in CV (Radford et al., 2021) and NLP (Devlin et al., 2019), researchers have developed EEG foundation models (EEG-FM) (Jiang et al., 2024b) to learn general representations from large-scale unlabeled EEG datasets. These models aim to overcome major obstacles in EEG analysis, including high inter-subject and intra-subject variability, and the scarcity of expertly annotated datasets (Rashid et al., 2020). While early works adapted architectures from other domains like BENDR (Kostas et al., 2021), recent studies focus on designing structures and pre-training strategies tailored to EEG characteristics, exemplified by CBraMod (Wang et al., 2024b), CSBrain (Zhou et al., 2025), and REVE (Ouahidi et al., 2025).

Despite the rapid progress of EEG-FMs, their **evaluation practices remain fragmented**. While foundation models aim for broad generalization among tasks and subjects, current evaluations often rely on task- or dataset-specific settings that contradict this goal. Existing studies benchmark models with inconsistent downstream datasets, preprocessing pipelines, and evaluation protocols, rendering cross-architecture comparisons unreliable and masking true pre-

training advances due to varying experimental setups (Lai et al., 2025). In practice, many methods compensate by introducing dataset-specific architectural and strategy tweaks, rather than learning representations that generalize across settings. For example, EEGPT (Wang et al., 2024a) freezes the backbone with linear probe, REVE (Ouahidi et al., 2025) employs two-stage fine-tuning, while CBraMod (Wang et al., 2024b) and CSBrain (Zhou et al., 2025) use fixed-size classifiers tailored to specific datasets. Moreover, existing **evaluations rarely go beyond end-task metrics**. Detailed technical analyses remain scarce, such as *gradient relations across datasets*, *evolution of intermediate representations during fine-tuning*, and *identifying components that drive knowledge transfer*. As a result, the mechanisms underlying pre-training efficacy remain unclear, particularly why scaling data often fails to yield proportional gains in downstream tasks (Jiang et al., 2024b).

Recent studies have benchmarked subject transfer (Wu et al., 2025) and adaptation techniques like LoRA (Hu et al., 2022) for EEG-FMs (Lee et al., 2025). However, several important aspects remain underexplored, including multi-task capability, classifier configuration, pretraining efficiency, and internal model dynamics such as gradient flow and feature representations. Therefore, a unified benchmark is required to ensure fair comparison and provide diagnostic analyses, replacing fragmented results with interpretable insights.

To address these issues, we introduce **EEG-FM-Bench**, a benchmark designed for the systematic and standardized evaluation of pretrained EEG-FMs. **The benchmark integrates various downstream tasks, unified data processing pipelines, consistent evaluation protocols, and a rich set of analytical and visualization tools**. All components are implemented within a unified open-source codebase to ensure reproducibility and fair comparison. Rather than optimizing for specific settings, this benchmark focuses on the general capabilities of EEG-FMs. Specifically, EEG-FM-Bench covers 14 datasets across 10 common EEG paradigms, including motor imagery, sleep staging, emotion recognition, disease diagnosis, and *etc*. It incorporates diverse configurations to assess pre-training quality and generalization: (1) **three fine-tuning strategies** (frozen-backbone, full-parameter, and LoRA (Hu et al., 2022)); (2) **two task setups** (single-task and multi-task); and (3) **three classifier configuration** (average pooling, attention pooling, and temporal-spatial-embedding dimension aggregation).

We evaluate seven pre-trained EEG-FMs and two general time-series models: BIOT (Yang et al., 2023), BENDR (Kostas et al., 2021), LaBraM (Jiang et al., 2024b), EEGPT (Wang et al., 2024a), CBraMod (Wang et al., 2024b), CSBrain (Zhou et al., 2025), REVE (Ouahidi et al., 2025), Mantis (Feofanov et al., 2025), and Moment (Goswami et al., 2024). To probe internal mecha-

nisms, our benchmark employs visualization and quantitative tools, measuring model behavior and optimization dynamics through gradient cosine similarity, subspace affinity, Centered Kernel Alignment (CKA) (Kornblith et al., 2019), and Representational Similarity Analysis (RSA) (Kriegeskorte et al., 2008). This integrated design enables both standardized benchmarking and diagnostic analysis, identifying how and why models succeed or fail across datasets.

Our evaluation on EEG-FM-Bench yields several key observations: 1) On fine-tuning strategies: A generalization gap emerges when using a frozen backbone, indicating that pre-trained representations often fail to transfer effectively to novel tasks; 2) On task setups: Multi-task learning acts as a powerful catalyst for knowledge sharing, overfitting alleviation for models that are not achievable in single-task settings; 3) On classifier configuration: Aggregating temporal, spatial, and embedding dimensions only outperforms pooling methods in motor imagery, and the overfitting issue remains in other tasks; 4) On optimization dynamics: Layer-wise analysis reveals that pre-training stabilizes the Transformer backbone, shifting the optimization burden to the input embedding, which bridges the domain gap between raw signals and latent features; 5) On pre-training efficiency: Despite aligning optimization trajectories, current methods suffer from low data utilization due to **objective misalignment** between reconstruction and classification, challenging the efficacy of pure data scaling. These findings inform future EEG-FM development, recommending a priority on pre-training efficiency (via model and objective design rather than mere data scaling), unified benchmarking to avoid fragmentation, and multi-task learning to reduce overfitting. Our contributions can be summarized as:

- We introduce **EEG-FM-Bench**, an open-source evaluation suite for EEG-FMs, integrating standardized protocols, diverse tasks, and diagnostic tools for end-to-end assessment.
- We conduct an empirical study on SOTA EEG-FMs, establishing baselines to compare their performance and generalization across various fine-tuning strategies.
- We analyze gradients and intermediate representations to identify pretraining bottleneck and architectural principles to inform future model and objective design.

## 2. Related Works

### 2.1. EEG Foundation Models

Early efforts adapt techniques from other fields; for instance, BENDR (Kostas et al., 2021) applies contrastive learning from speech processing, while others focus on masked signal modeling. These include BrainBERT (Wang et al., 2023), which operates on EEG spectrograms, and EEG2Rep (Mohammadi Foumani et al., 2024) and

Brant (Zhang et al., 2023), which perform masking in the latent space. Regarding input tokenization, BIOT (Yang et al., 2023) introduces channel-independent methods for variable inputs, while LaBraM (Jiang et al., 2024b) and EEGFormer (Wan et al., 2023) utilize vector-quantized approaches for raw and frequency-domain signals. In terms of architecture, EEGPT (Wang et al., 2024a) integrates spatio-temporal alignment, CBraMod (Wang et al., 2024b) uses criss-cross attention, and CSBrain (Zhou et al., 2025) proposes a cross-scale structure. REVE (Ouahidi et al., 2025) scales up pre-training, refining objectives using layer-wise features and employing 4D positional encodings. Furthermore, models like Brant-2 (Yuan et al., 2024) combine scalp with intracranial EEG, while LEAD (Wang et al., 2025) targets clinical challenges such as Alzheimer’s disease. This rapid evolution complicates fair comparisons between approaches, highlighting the need for standardized benchmarks to evaluate and analyze progress.

## 2.2. EEG Benchmarks

The BCI and broader EEG analysis communities contend with a reproducibility crisis, partly due to a lack of unifying standards. Early efforts, such as BCI competitions, provide public datasets and standardized metrics. Recent competitions continue this trend; for instance, BEETL (Wei et al., 2022) emphasizes transfer learning, while the EEG Foundation Challenge (Aristimunha et al., 2025) focuses on cross-subject cognitive tasks, though limited to the HBN dataset. MOABB (Jayaram & Barachant, 2018) offers an open-source evaluation platform, yet its scope restricts to specific paradigms like motor imagery, SSVEP, and P300. Other benchmarks target specific tasks or architectures, including denoising (EEGdenoiseNet (Zhang et al., 2021)), emotion recognition (LibEER (Liu et al., 2024)), Parkinson’s diagnosis (Avola et al., 2025), and GNNs (GNN4EEG (Zhang et al., 2024)). Specifically for EEG-FMs, AdaBrain-Bench (Wu et al., 2025) and Lee et al. (2025) benchmark subject transfer and adaptation techniques. However, these studies overlook critical aspects, including multi-task capability, classifier configuration, pre-training efficiency, and internal dynamics such as gradient flow. Consequently, a unified benchmark for current EEG-FMs is lacking. Such a resource is necessary to ensure reproducibility and provide a fair basis for comparing methodological innovations.

## 3. Benchmark Pipeline

Fig. 2 provides an overview of the EEG-FM-Bench. Designed for fair, reproducible, and diagnostic evaluation, the system comprises three core modules: **Data Management**, **Configurable Evaluation**, and **Diagnostic Analyses**. It employs a modular open-source structure with unified abstractions for datasets, backbones, classifiers, and training

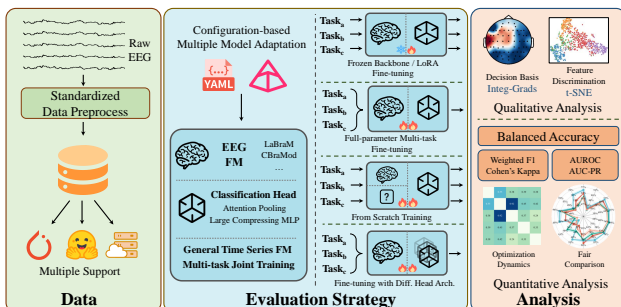


Figure 2. Overview of the EEG-FM-Bench framework. **Data Management:** A unified pipeline standardizes preprocessing across 14 datasets covering 10 canonical EEG paradigms. **Configurable Evaluation:** A configuration-based system facilitates flexible assessments by decoupling model backbones from decoder heads, supporting diverse fine-tuning strategies (e.g., frozen-backbone, LoRA, multi-task). **Diagnostic Analyses:** The platform provides both qualitative visualizations (e.g., decision basis, feature discrimination) and quantitative metrics to examine model performance and optimization dynamics.

setups, ensuring that different EEG-FMs are evaluated under *matched* preprocessing and optimization conditions. Extending beyond downstream accuracy, the pipeline supports **fine-tuning dynamics** by coupling gradient-space geometry with representation-space similarity, enabling controlled comparisons across model initialization (scratch v.s. pre-trained), training phrase (pre-train v.s. fine-tune), training regime (single-task v.s. multi-task), and model component (patching v.s. transformer).

### 3.1. Data Management

**Task and Dataset Curation.** Our benchmark incorporates 14 public datasets covering 10 canonical EEG paradigms, including motor imagery (BCIC-2a, PhysioMI, Mimul-11), emotion recognition (SEED, SEED-V, SEED-VII), sleep stage classification (HMC), seizure detection (Siena), mental stress assessment (Workload), abnormal detection (TUAB), event type classification (TUEV), visual target detection (Things-EEG-2), Alzheimer’s Disease recognition (ADFTD), and slowing event classification (TUSL) (see Appx. A for more details). Through these diverse datasets, EEG-FM-Bench serves both as a ranking tool and a diagnostic instrument to identify architectural and representational weaknesses. The framework features an extensible API, enabling the integration of custom datasets and user-defined data assembly configurations.

**Standardized Data Processing.** Since inconsistent processing leads to incomparable results, we implement a standardized pipeline applied across datasets. This pipeline comprises the following steps (see Appx. B.1 for details): **1. Selection:** The system selects data based on specified event markers and channel sets. **2. Filtering:** A band-pass filter (0.1–100 Hz) and a notch filter (50 or 60 Hz) remove noise while preserving signal information. **3. Resampling:** Sig-

nals are downsampled to model-specific target rates based on their pretraining setting. **4. Segmentation:** Continuous data is segmented into fixed-length windows (*e.g.*, 4-second trials) and assigned to splits based on task-specific rules. **5. Splitting:** Datasets are partitioned into three splits using a subject-independent strategy while preserving label distribution. For emotion recognition, a subject-dependent strategy aligns with common protocols. **6. Formatting:** Processed samples are saved in efficient formats (“Parquet” for storage, “Arrow” for accelerated loading).

### 3.2. Configurable Evaluation

We evaluate pre-trained EEG-FMs by structuring the design into three dimensions: **fine-tuning strategy**, **task setup**, and **classifier head**, which allows controlled ablations on adaptability, transfer, and decoding inductive bias, while keeping data processing and optimization across models. **Fine-tuning strategies.** We consider three strategies that probe different levels of parameter adaptation:

- **Frozen-backbone.** Only the classifier head is trained while the backbone remains frozen. This evaluates the intrinsic quality of pre-trained representations.
- **Full-parameter.** All model parameters are fine-tuned on downstream data, assessing how effectively pre-trained features adapt to the target task distribution.
- **Parameter-efficient.** The backbone is fine-tuned using LoRA, enabling efficient adaptation with fewer trainable parameters and reduced memory footprint.

**Task setups.** To evaluate both within-task adaptation and cross-task knowledge sharing, each fine-tuning strategy can be instantiated under two task setups:

- **Single-task setting.** The model is fine-tuned and evaluated on one downstream dataset at a time, reflecting the standard pre-training transfer protocol.
- **Multi-task setting.** The model is fine-tuned on a mixture constructed from all downstream tasks, evaluating whether joint training improves generalization and benefits each paradigm. We employ resampling to mitigate dataset imbalance and stabilize optimization.

**Classifier heads.** To decouple backbone capability from decoding inductive bias, we implement three classifier heads:

- **MLP with patch average pooling.** We average pool patch-level features and apply an MLP classifier.
- **MLP with dimension compression.** We apply a large MLP that reduces temporal, spatial, and embedding, testing whether a high-capacity improves performance.
- **MLP with attention pooling.** We use attention pooling to aggregate patches into a global representation, enabling adaptive weighting and improving performance when discriminative features are sparse.

### 3.3. Diagnostic Analyses

We provide both **standard performance evaluation** and **diagnostic analysis** of fine-tuning dynamics.

**Performance Metrics.** To address class imbalance, we select metrics including Balanced Accuracy, Weighted F1, AUROC, AUC-PR, and Cohen’s Kappa (see Appx. B.4 for detailed definition). Within our benchmark, Balanced Accuracy is used for all classification task, AUROC and AUC-PR are used for binary classification tasks, and Cohen’s Kappa and Weighted F1 are used to multi-class classification tasks.

**Fine-tuning Dynamics Analysis.** We analyze fine-tuning dynamics by linking *gradient-space geometry* with *representation-space similarity* across four settings: (1) initialization (scratch vs. pre-trained); (2) phase (pre-training vs. fine-tuning); (3) regime (single-task vs. multi-task); and (4) component (patching vs. transformer). At designated intervals, we collect parameter gradients and extract intermediate layer representations via forward hooks on fixed probe batches. To reduce memory overhead and ensure consistent comparisons, we compress gradients and features using CountSketch (Charikar et al., 2004) hashing projector, followed by  $\ell_2$ -normalization.

**Gradient-space analysis.** For each parameter group and each condition (initialization, dataset or training parse), we compute alignment measures by cosine similarity between projected gradient directions:  $\cos(\mathbf{g}_a, \mathbf{g}_b) = \frac{\langle \mathbf{g}_a, \mathbf{g}_b \rangle}{\|\mathbf{g}_a\|_2 \|\mathbf{g}_b\|_2}$ . To capture the dominant subspace structure of optimization directions, we compute subspace affinity. For each condition, we construct a gradient matrix, apply PCA, and average the top singular values of the projection matrix  $U^\top V: A = U^\top V$ ,  $\text{Affinity} = \frac{1}{k} \sum_{i=1}^k \sigma_i(A)$ , where  $U$  and  $V$  denote the  $k$ -dimensional orthonormal bases for two conditions, and  $\sigma_i(\cdot)$  is the  $i$ -th singular value.

We further quantify gradient conflicts using a metric inspired by PCGrad (Yu et al., 2020). For paired conditions, we compare gradients at aligned steps, identifying conflicts where the cosine similarity is negative:  $\text{Conflict} = \mathbb{I}[\cos(\mathbf{g}_a, \mathbf{g}_b) < 0]$ . Conflict frequency is the empirical mean over samples, while the mean conflict angle is derived from these negative cosine values.

We also analyze the distribution of gradient energy across parameter groups. The energy proportion  $E_{\text{axis}, G}$  for a specific condition and parameter group  $G$  is defined as:

$$E_{\text{axis}, G} = \frac{\sum_t \|\mathbf{g}_{\text{axis}, G}^{(t)}\|_2^2}{\sum_{G' \in \mathcal{G}} \sum_t \|\mathbf{g}_{\text{axis}, G'}^{(t)}\|_2^2}, \quad (1)$$

where  $\mathcal{G}$  is the set of all parameter groups, and  $t$  denotes the training step. This distribution highlights which parameter groups dominate the gradient updates.

**Representation-space analysis.** Representations are extracted from model layers using fixed probe batches, with

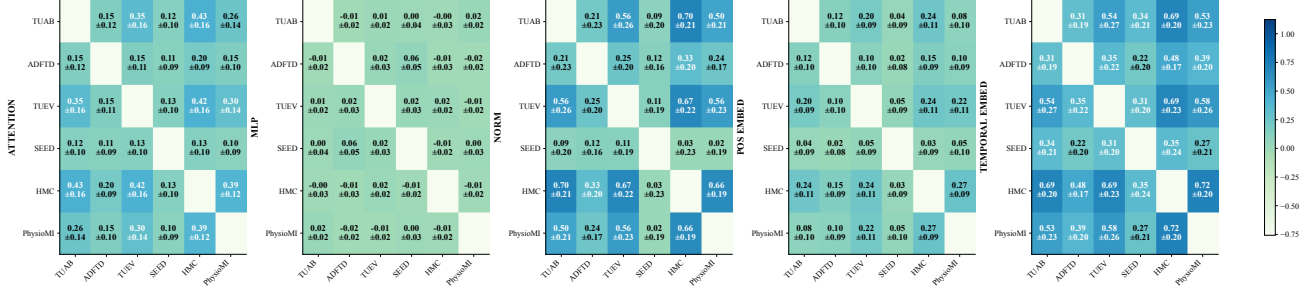


Figure 3. Cross-task gradient correlation analysis. The heatmaps visualize the pairwise cosine similarity of gradients between different tasks across specific model components, revealing how tasks interact during optimization. Best viewed via zoom-in.

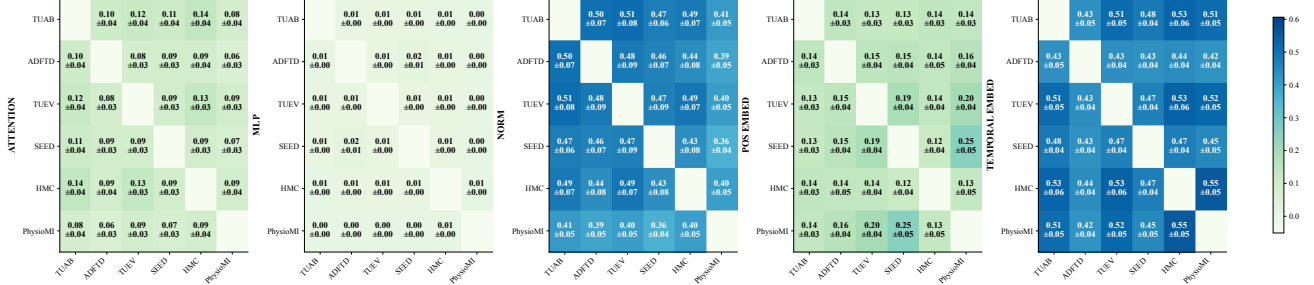


Figure 4. Cross-task subspace affinity analysis. This metric quantifies the geometric alignment of optimization subspaces among tasks, indicating the extent to which different tasks share a common optimization direction within each component. Best viewed via zoom-in.

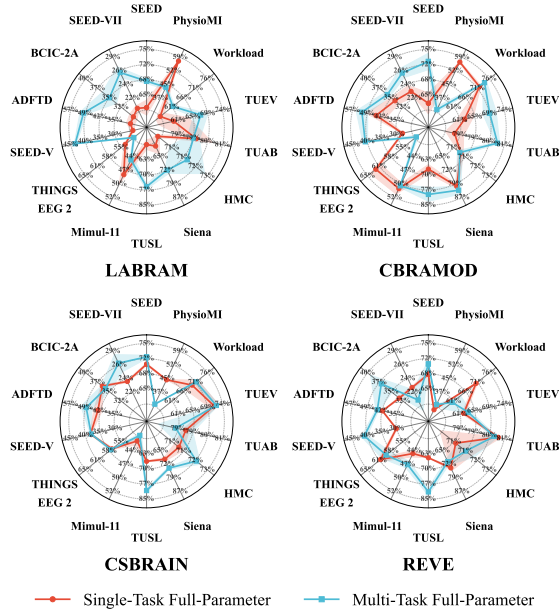


Figure 5. Performance comparison between single-task and multi-task fine-tuning on 14 downstream tasks. Best viewed via zoom-in.

their similarity quantified via Centered Kernel Alignment (CKA) and Representational Similarity Analysis (RSA). For CKA, we compute linear kernels  $K_X = XX^\top$  and  $K_Y = YY^\top$  for representations  $X, Y \in \mathbb{R}^{n \times d}$ , where  $n$  is the sample size and  $d$  is the feature dimension. We then calculate the Hilbert-Schmidt Independence Criterion (HSIC) (Freiwald & Tsao, 2010) using the centering matrix

$$H = I_n - \frac{1}{n} \mathbf{1}_n \mathbf{1}_n^\top \quad (\mathbf{1}_n \text{ is an } n\text{-dimensional vector of ones):}$$

$$\text{HSIC}(K_X, K_Y) = \frac{1}{(n-1)^2} \text{tr}(K_X H K_Y H), \quad (2)$$

where  $\text{tr}(\cdot)$  denotes the matrix trace operator. CKA normalizes HSIC to achieve scale invariance:

$$\text{CKA}(X, Y) = \frac{\text{HSIC}(K_X, K_Y)}{\sqrt{\text{HSIC}(K_X, K_X) \cdot \text{HSIC}(K_Y, K_Y)}}. \quad (3)$$

RSA quantifies the similarity of representations from two models via representational dissimilarity matrices (RDMs). For a representation matrix  $X \in \mathbb{R}^{n \times d}$ , we compute the RDM using sample-wise Pearson correlation:

$$\text{RDM}_{ij} = 1 - \text{corr}_{\text{Pear}}(x_i, x_j). \quad (4)$$

We extract the upper triangular elements of the RDMs and compute the Spearman correlation between them:

$$\text{RSA}(X, Y) = \text{Corr}_{\text{Spear}}(\text{vec}(\text{RDM}_X), \text{vec}(\text{RDM}_Y)). \quad (5)$$

This provides a similarity metric for layer-wise or condition-aware feature evolvment comparison.

**Probing protocol.** All analyses are conducted during *fine-tuning with fixed budget*. Every  $n$  steps, we probe gradients and representations using pre-sampled batches fixed throughout the run. This ensures consistent inputs for comparisons across optimization process and conditions (e.g., scratch vs. pre-trained). We repeat the procedure across 10 random seeds and report aggregated statistics.

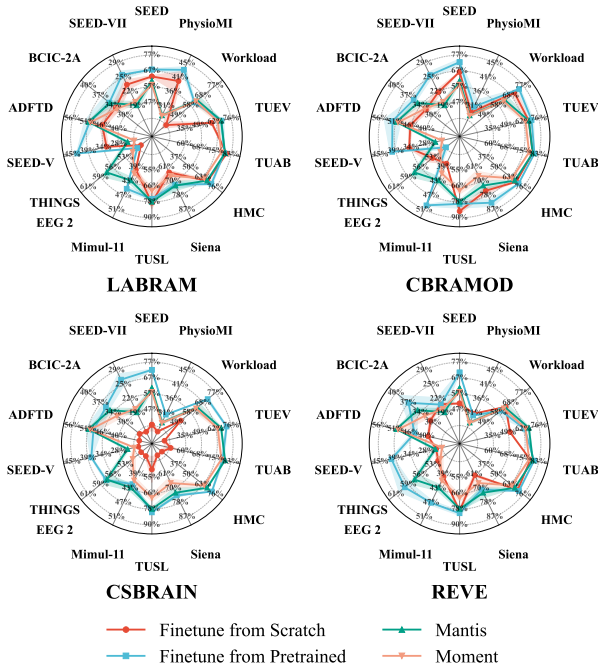


Figure 6. Performance comparison between fine-tuning from scratch (red) and from pre-trained model (blue). General time-series models are included for reference. Best viewed via zoom-in.

## 4. Experiment and Analysis

### 4.1. Experiment Setup

All models are evaluated within the EEG-FM-Bench framework. For each experiment, a classifier head is attached to the EEG-FM for downstream tasks. We report the mean and standard deviation across five independent runs with different random seeds. For analysis, we use 32 fixed batches to probe gradients and intermediate representations throughout the training budget. Unless otherwise mentioned, all the results are reported under multi-task, full-parameter, average pooling decoder with pretrained EEG-FMs. **See Appx. B for implementation details; Appx. C, D for detailed results and analysis; Appx. E for detailed visualization.**

### 4.2. Impact of Task Organization

**Performance Comparison.** Standard fine-tuning isolates downstream datasets, often missing cross-task knowledge sharing. Therefore, we compare two strategies: (1) **Single-Task**, where models are fine-tuned on each dataset individually; and (2) **Multi-Task**, where models are fine-tuned jointly on a mixture of all tasks. Fig. 5 presents the performance comparison across four representative models using radar charts. First, multi-task learning (blue) consistently matches or outperforms single-task settings (red) across most datasets. Single-task models frequently overfit on specific datasets (*e.g.*, ADFTD, TUEV), whereas multi-task learning acts as a regularizer, utilizing diverse distributions

to stabilize optimization. Second, negative transfer occurs in conflicting paradigms. In motor imagery and visual tasks, single-task baselines occasionally prevail, suggesting caution in task grouping under large domain discrepancies.

**Mechanism Analysis: Gradient and Subspace Dynamics.** We examine optimization dynamics via gradient alignment and feature space geometry to explain the multi-task generalizability. Using LaBraM (others in Appx. D) as a case, we compute inter-task gradient **Correlation** and **Subspace Affinity** across model components. Figures 3 and 4 show that **Normalization** and **Temporal Embedding** layers exhibit consistently high gradient correlations. This suggests these components learn task-agnostic temporal dynamics shared across datasets. Conversely, **MLP** and **Attention** layers show lower affinity, implying they capture task-specific patterns. High correlation in shared components aligns optimization of fundamental extractors, preventing the model from collapsing into task-specific local minima. Thus, we recommend multi-task joint training as a default strategy for stability, especially for limited data.

### 4.3. Impact of Pre-training

**Performance Benchmarking: EEG-FMs vs. Time-FMs.** We evaluate pre-training utility by comparing three paradigms: scratch, pre-trained checkpoints, and general time-series models (Mantis, Moment). As shown in Fig. 6, pre-training (blue) consistently outperforms scratch (red) across most datasets, especially on complex tasks like SEED-V and BCIC-2A. This confirms that pre-training provides a superior initialization. However, general time-series models achieve competitive performance in some tasks despite using non-EEG training data.

**Optimization Dynamics.** We visualize LaBraM’s training dynamics to explain pre-training advantages. We monitor gradient norms and representational similarity every 16 steps on a controlled fine-tuning subset. Fig. 7 (left) shows the gradient norm intensity. In *Pre-trained* settings, optimization focuses on the Temporal Embedding (green area), while the backbone (Attention, MLP, Norm) remains stable. In contrast, *Scratch* requires intensive optimization across all components. This indicates pre-training stabilizes the Transformer backbone for sequence modeling. Therefore, fine-tuning primarily adapts the Temporal Embedding to bridge the gap between raw signals and latent space. Figs. 7 (mid) and (right) track representational evolution via CKA and RSA, showing progressively increasing alignment scores among fine-tuning. CKA shows strengthening structural correspondence, while RSA indicates converging sample geometry. Therefore, the multi-task fine-tuning acts as an attractor, guiding the scratch model to align representations with the pre-trained model, validating the robustness of the learned features. Notably, CSBrain tends to collapse under the scratch setting (see Appx. D for detailed analysis).

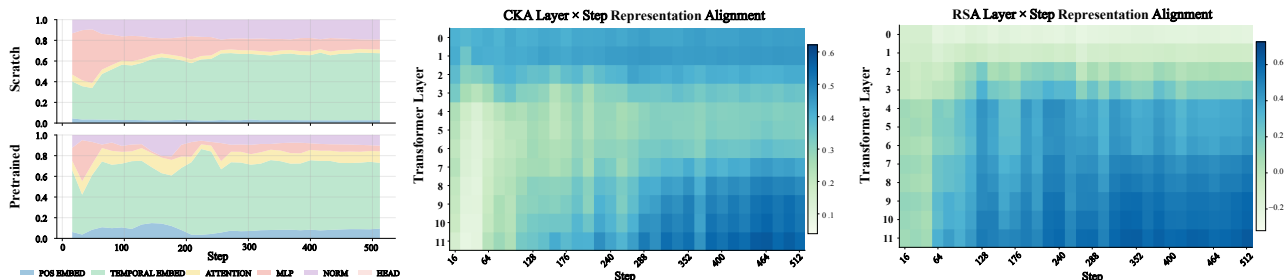


Figure 7. Evolution of optimization dynamics during fine-tuning. Left: Relative gradient norm intensity across modules for Scratch vs. Pre-trained settings. Mid and Right: Layer-wise CKA and RSA between Scratch and Pre-trained models over training steps, showing representational convergence. Best viewed via zoom-in.

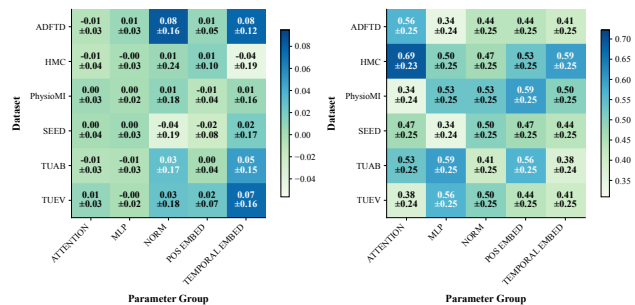


Figure 8. Gradient alignment between pre-training and downstream tasks. Left: Cosine similarity of gradients derived from Reconstruction and Classification losses. Right: Probability of gradient conflicts (sign disagreement). Best viewed via zoom-in.

**Inefficiency in Pre-training: Gradient Analysis.** Performance gains of EEG-FMs are often not proportional to the pre-training data scale. We investigate this inefficiency by analyzing gradient alignment between pre-training (Masked Reconstruction, MSE) and downstream (Classification, Cross-Entropy) objectives on identical samples. To avoid high-dimensional orthogonality, we project gradients to a low-dimensional space ( $d = 6$ ) via CountSketch before computing correlations. Fig. 8 (right) shows near-zero or negative gradient correlations across most datasets. Furthermore, Fig. 8 (left) reveals a high probability of gradient conflict (blue blocks). The high variance and misalignment imply that reconstruction optimization is disjoint or conflicting with semantic classification. Current pre-training functions primarily as a “time-series aware initialization” rather than effective knowledge transfer. Given EEG’s low signal-to-noise ratio, scaling reconstruction yields diminishing returns; thus, developing objectives or modules that capture discriminative features is critical.

#### 4.4. Impact of Fine-tuning Strategies

We compare three adaptation strategies, Frozen, LoRA, and Full-parameter, across four EEG-FMs (Fig. 9). First, Full-parameter fine-tuning (green) consistently yields the highest performance in most of datasets, establishing the upper bound for adaptation. Second, the Frozen backbone (red)

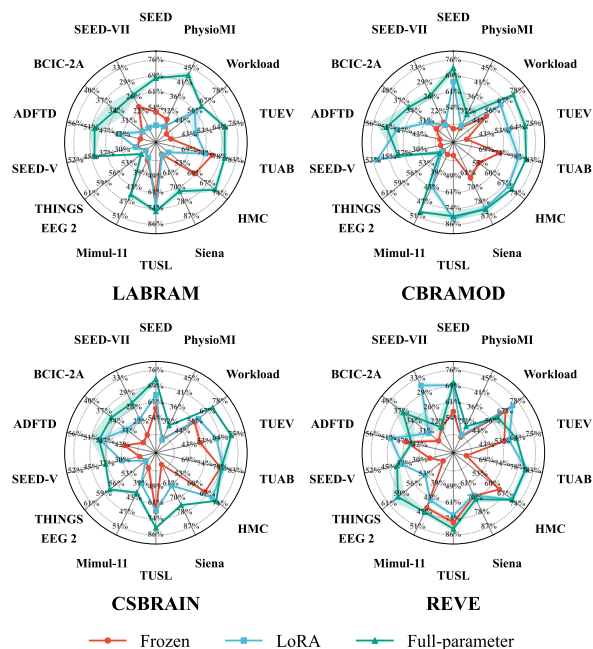


Figure 9. Performance comparison among fine-tuning strategies.

suffers from a severe **generalization gap**; the sharp drop indicates fixed representations lack sufficient discriminability for direct transfer. Third, LoRA (blue) offers an efficient alternative but performance varies by base model. We observe that LoRA performs competitively in models where pre-training demonstrates a significant advantage over scratch (e.g., CbBraMod and REVE), whereas it struggles in weaker baselines. This implies parameter-efficient tuning relies heavily on the backbone’s quality.

#### 4.5. Impact of Classifier Head

We examine the decoder head by comparing three configurations: Average Pooling, Large Compressing MLP, and Attention Pooling (Fig. 10). The comparison reveals a capacity-stability trade-off. **Average Pooling** (red) delivers the most balanced performance; its simplicity acts as regularization, mitigating overfitting to noisy EEG data. Conversely, high-capacity decoders like **Attention Pooling** and

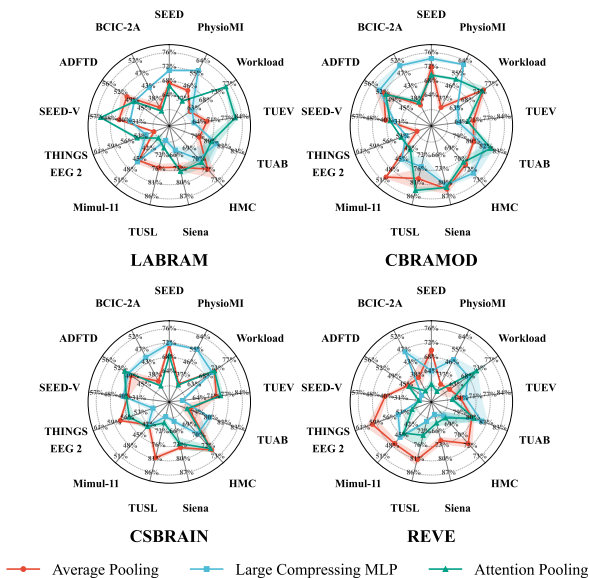


Figure 10. Performance comparison among classifier heads.

MLP show higher variance and a tendency to overfit on simpler tasks. However, the **Large Compressing MLP** (blue) excels in Motor Imagery tasks (*e.g.*, PhysioMI, BCIC-2A). This suggests preserving high-dimensional embeddings captures fine-grained signal fluctuations and temporal dynamics otherwise smoothed out by global pooling. Therefore, rather than increasing decoder complexity, future research should prioritize refining the Foundation Model’s architecture to generate comprehensive representations, reducing the burden on downstream classifiers.

#### 4.6. Overall Benchmarking and Scaling Analysis

We synthesize the performance of seven EEG-FMs and two general time-series models in Fig. 11 and Fig. 1. The comparative analysis yields critical insights regarding the relationship between scale and performance. EEGPT is the top-performing model, achieving the highest average balanced accuracy across the benchmark. Closely following is CBraMod, delivering comparable performance to EEGPT while maintaining remarkable efficiency with only 4.92M parameters, roughly 1/5 the size of EEGPT and 1/14 of REVE. In stark contrast, REVE, despite possessing the largest model capacity (69.19M) and utilizing the most extensive pre-training corpus ( $> 10^4$  GB), fails to surpass these compact models. This deviation from typical scaling laws suggests that in the low signal-to-noise ratio EEG domain, architectural inductive bias (*e.g.*, EEGPT’s cascade structure or CBraMod’s dual-branch design) outweighs raw data scale and parameter count. Furthermore, specialized EEG-FMs consistently outperform general time-series baselines; notably, Moment holds 35M parameters but achieves the lowest accuracy, validating the necessity of domain-specific pre-training over generic temporal modeling.

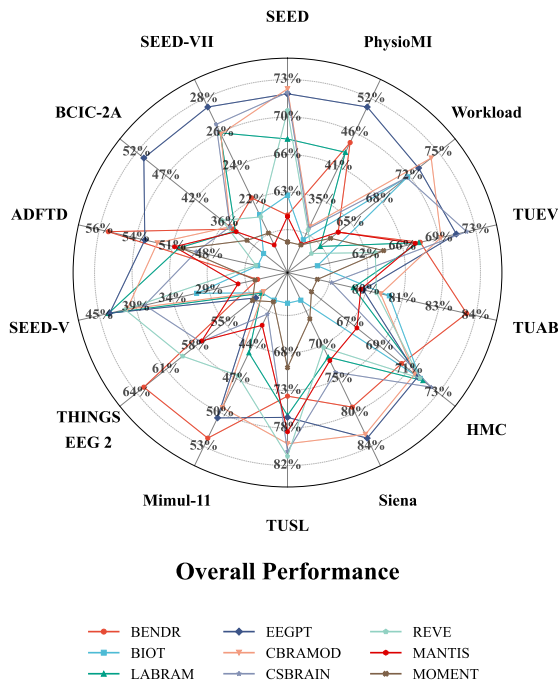


Figure 11. Holistic performance comparison of seven EEG-FMs and two Time-FMs across 14 datasets. Best viewed via zoom-in.

## 5. Conclusion and Future Perspectives

In this work, we introduce EEG-FM-Bench, a standardized benchmark for EEG-FMs, establishing baselines for seven EEG-FMs and two general time-series models across 14 datasets and 10 paradigms. We identify a significant generalization gap in frozen-backbone settings, indicating that current masked reconstruction objectives fail to produce sufficiently discriminative representations for downstream tasks. Our results challenge typical scaling laws, showing that compact architectures with domain-specific inductive biases outperform larger models trained on vast datasets, proving that efficient design currently outweighs parameter scaling in the low signal-to-noise EEG domain. Furthermore, multi-task learning acts as an effective regularizer, mitigating overfitting and enhancing robustness by leveraging diversity across EEG paradigms.

Based on these findings, we propose three directions for future research. First, **rethinking pre-training objectives** is necessary to resolve the gradient conflict between reconstruction and downstream classification, moving towards methods that capture discriminative semantic features. Second, developing **neuro-informed architectures** that explicitly model brain connectivity is crucial for learning physiologically grounded representations rather than relying on brute-force scaling. Finally, **embracing multi-task and multi-modal learning** is recommended to maximize data utilization, integrating complementary signals to construct generalized models of brain function.

## Impact Statement

This paper presents work whose goal is to advance the field of machine learning. There are many potential societal consequences of our work, none of which we feel must be specifically highlighted here.

## References

- Alvarez-Estevéz, D. and Rijsman, R. M. Inter-database validation of a deep learning approach for automatic sleep scoring. *PLOS ONE*, 16(8):1–27, 08 2021.
- Aristimunha, B., Truong, D., Guetschel, P., Shirazi, S. Y., Guyon, I., Franco, A. R., Milham, M. P., Dotan, A., Makeig, S., Gramfort, A., et al. Eeg foundation challenge: From cross-task to cross-subject eeg decoding. *arXiv preprint arXiv:2506.19141*, 2025.
- Avola, D., Bernardini, A., Crocetti, G., Ladogana, A., Lezoche, M., Mancini, M., Pannone, D., and Ranaldi, A. Benchmarking of eeg analysis techniques for parkinson’s disease diagnosis: A comparison between traditional ml methods and foundation dl methods, 2025.
- Charikar, M., Chen, K., and Farach-Colton, M. Finding frequent items in data streams. *Theoretical Computer Science*, 312(1):3–15, 2004. ISSN 0304-3975. Automata, Languages and Programming.
- Deti, P., Vatti, G., and Zabalo Manrique de Lara, G. Eeg synchronization analysis for seizure prediction: A study on data of noninvasive recordings. *Processes*, 8(7), 2020.
- Devlin, J., Chang, M.-W., Lee, K., and Toutanova, K. Bert: Pre-training of deep bidirectional transformers for language understanding. In *NAACL*, pp. 4171–4186, 2019.
- Feofanov, V., Wen, S., Alonso, M., Ilbert, R., Guo, H., Tiomoko, M., Pan, L., Zhang, J., and Redko, I. Mantis: Lightweight calibrated foundation model for user-friendly time series classification. *arXiv preprint arXiv:2502.15637*, 2025.
- Freiwald, W. A. and Tsao, D. Y. Functional compartmentalization and viewpoint generalization within the macaque face-processing system. *Science*, 330(6005):845–851, 2010.
- Gifford, A. T., Dwivedi, K., Roig, G., and Cichy, R. M. A large and rich eeg dataset for modeling human visual object recognition. *NeuroImage*, 264:119754, 2022.
- Goswami, M., Szafer, K., Choudhry, A., Cai, Y., Li, S., and Dubrawski, A. Moment: A family of open time-series foundation models. *arXiv preprint arXiv:2402.03885*, 2024.
- Gramfort, A., Luessi, M., Larson, E., Engemann, D. A., Strohmeier, D., Brodbeck, C., Goj, R., Jas, M., Brooks, T., Parkkonen, L., and Hämäläinen, M. Meg and eeg data analysis with mne-python. *Frontiers in Neuroscience*, 7, 2013.
- Harati, A., Golmohammadi, M., Lopez, S., Obeid, I., and Picone, J. Improved eeg event classification using differential energy. In *SPMB*, pp. 1–4, 2015.
- Hu, E. J., Shen, Y., Wallis, P., Allen-Zhu, Z., Li, Y., Wang, S., Wang, L., Chen, W., et al. Lora: Low-rank adaptation of large language models. *ICLR*, 1(2):3, 2022.
- Jayaram, V. and Barachant, A. Moabb: trustworthy algorithm benchmarking for bcis. *Journal of neural engineering*, 15(6):066011, 2018.
- Jeong, J.-H., Cho, J.-H., Shim, K.-H., Kwon, B.-H., Lee, B.-H., Lee, D.-Y., Lee, D.-H., and Lee, S.-W. Multimodal signal dataset for 11 intuitive movement tasks from single upper extremity during multiple recording sessions. *GigaScience*, 9(10):giaa098, 2020.
- Jiang, W.-B., Liu, X.-H., Zheng, W.-L., and Lu, B.-L. Seed-vii: A multimodal dataset of six basic emotions with continuous labels for emotion recognition. *IEEE Transactions on Affective Computing*, 2024a.
- Jiang, W.-B., Zhao, L.-M., and Lu, B.-L. Large brain model for learning generic representations with tremendous eeg data in bci. *arXiv preprint arXiv:2405.18765*, 2024b.
- Kornblith, S., Norouzi, M., Lee, H., and Hinton, G. Similarity of neural network representations revisited. In *International conference on machine learning*, pp. 3519–3529. PMIR, 2019.
- Kostas, D., Aroca-Ouellette, S., and Rudzicz, F. Bendr: Using transformers and a contrastive self-supervised learning task to learn from massive amounts of eeg data. *Frontiers in Human Neuroscience*, 15:653659, 2021.
- Kriegeskorte, N., Mur, M., and Bandettini, P. A. Representational similarity analysis-connecting the branches of systems neuroscience. *Frontiers in systems neuroscience*, 2:249, 2008.
- Lai, J., Wei, J., Yao, L., and Wang, Y. A simple review of eeg foundation models: Datasets, advancements and future perspectives. *arXiv preprint arXiv:2504.20069*, 2025.
- Lee, N., Barmpas, K., Panagakakis, Y., Adamos, D., Laskaris, N., and Zafeiriou, S. Are large brainwave foundation models capable yet? insights from fine-tuning. *arXiv preprint arXiv:2507.01196*, 2025.

- Liu, H., Yang, S., Zhang, Y., Wang, M., Gong, F., Xie, C., Liu, G., Liu, Z., Liu, Y.-J., Lu, B.-L., et al. Libeer: A comprehensive benchmark and algorithm library for eeg-based emotion recognition. *arXiv preprint arXiv:2410.09767*, 2024.
- Liu, W., Qiu, J.-L., Zheng, W.-L., and Lu, B.-L. Comparing recognition performance and robustness of multimodal deep learning models for multimodal emotion recognition. *IEEE TCDS*, 14(2):715–729, 2022.
- López, S., Suarez, G., Jungreis, D., Obeid, I., and Picone, J. Automated identification of abnormal adult eegs. In *SPMB*, pp. 1–5, 2015.
- Maaten, L. v. d. and Hinton, G. Visualizing data using t-sne. *Journal of machine learning research*, 9(Nov):2579–2605, 2008.
- Miltiadous, A., Tzimourta, K. D., Afrantou, T., Ioannidis, P., Grigoriadis, N., Tsalikakis, D. G., Angelidis, P., Tsipouras, M. G., Glavas, E., Giannakeas, N., et al. A dataset of scalp eeg recordings of alzheimer’s disease, frontotemporal dementia and healthy subjects from routine eeg. *Data*, 8(6):95, 2023.
- Mohammadi Foumani, N., Mackellar, G., Ghane, S., Irtza, S., Nguyen, N., and Salehi, M. Eeg2rep: enhancing self-supervised eeg representation through informative masked inputs. In *Proceedings of the 30th ACM SIGKDD Conference on Knowledge Discovery and Data Mining*, pp. 5544–5555, 2024.
- Ouahidi, Y. E., Lys, J., Thölke, P., Farrugia, N., Padeloup, B., Gripon, V., Jerbi, K., and Lioi, G. Reve: A foundation model for eeg - adapting to any setup with large-scale pretraining on 25,000 subjects. *ArXiv*, abs/2510.21585, 2025.
- Radford, A., Kim, J. W., Hallacy, C., Ramesh, A., Goh, G., Agarwal, S., Sastry, G., Askell, A., Mishkin, P., Clark, J., et al. Learning transferable visual models from natural language supervision. In *International conference on machine learning*, pp. 8748–8763. PmLR, 2021.
- Ramantani, G., Maillard, L., and Koessler, L. Correlation of invasive eeg and scalp eeg. *Seizure*, 41:196–200, 2016.
- Rashid, M., Sulaiman, N., PP Abdul Majeed, A., Musa, R. M., Ab. Nasir, A. F., Bari, B. S., and Khatun, S. Current status, challenges, and possible solutions of eeg-based brain-computer interface: a comprehensive review. *Frontiers in neurorobotics*, 14:25, 2020.
- Schalk, G., McFarland, D., Hinterberger, T., Birbaumer, N., and Wolpaw, J. Bci2000: a general-purpose brain-computer interface (bci) system. *IEEE TBE*, 51(6):1034–1043, 2004.
- Sundararajan, M., Taly, A., and Yan, Q. Axiomatic attribution for deep networks. In *International conference on machine learning*, pp. 3319–3328. PMLR, 2017.
- Van Den Oord, A., Vinyals, O., et al. Neural discrete representation learning. In *NeurIPS*, 2017.
- von Weltin, E., Ahsan, T., Shah, V., Jamshed, D., Golmohammadi, M., Obeid, I., and Picone, J. Electroencephalographic slowing: A primary source of error in automatic seizure detection. In *SPMB*, pp. 1–5, 2017.
- Wan, Z., Li, M., Liu, S., Huang, J., Tan, H., and Duan, W. Eegformer: A transformer-based brain activity classification method using eeg signal. *Frontiers in neuroscience*, 17:1148855, 2023.
- Wang, C., Subramaniam, V., Yaari, A. U., Kreiman, G., Katz, B., Cases, I., and Barbu, A. Brainbert: Self-supervised representation learning for intracranial recordings. *arXiv preprint arXiv:2302.14367*, 2023.
- Wang, G., Liu, W., He, Y., Xu, C., Ma, L., and Li, H. Eegpt: Pretrained transformer for universal and reliable representation of eeg signals. *Advances in Neural Information Processing Systems*, 37:39249–39280, 2024a.
- Wang, J., Zhao, S., Luo, Z., Zhou, Y., Jiang, H., Li, S., Li, T., and Pan, G. Cbramod: A criss-cross brain foundation model for eeg decoding. *arXiv preprint arXiv:2412.07236*, 2024b.
- Wang, Y., Huang, N., Mammone, N., Cecchi, M., and Zhang, X. Lead: Large foundation model for eeg-based alzheimer’s disease detection. *arXiv preprint arXiv:2502.01678*, 2025.
- Wei, X., Faisal, A. A., Grosse-Wentrup, M., Gramfort, A., Chevallier, S., Jayaram, V., Jeunet, C., Bakas, S., Ludwig, S., Barmpas, K., et al. 2021 beetl competition: Advancing transfer learning for subject independence and heterogeneous eeg data sets. In *NeurIPS 2021 Competitions and Demonstrations Track*, pp. 205–219. PMLR, 2022.
- Wu, J., Ren, Z., Wang, J., Zhu, P., Song, Y., Liu, M., Zheng, Q., Bai, L., Ouyang, W., and Song, C. Adabrainbench: Benchmarking brain foundation models for brain-computer interface applications. *ArXiv*, abs/2507.09882, 2025.
- Yang, C., Westover, M., and Sun, J. Biot: Biosignal transformer for cross-data learning in the wild. *Advances in Neural Information Processing Systems*, 36:78240–78260, 2023.
- Yu, T., Kumar, S., Gupta, A., Levine, S., Hausman, K., and Finn, C. Gradient surgery for multi-task learning. *Advances in neural information processing systems*, 33:5824–5836, 2020.

- Yuan, Z., Zhang, D., Chen, J., Gu, G., and Yang, Y. Brant-2: Foundation model for brain signals. *CoRR*, 2024.
- Zhang, D., Yuan, Z., Yang, Y., Chen, J., Wang, J., and Li, Y. Brant: Foundation model for intracranial neural signal. *Advances in Neural Information Processing Systems*, 36: 26304–26321, 2023.
- Zhang, H., Zhao, M., Wei, C., Mantini, D., Li, Z., and Liu, Q. Eegdenoisenet: a benchmark dataset for deep learning solutions of eeg denoising. *Journal of Neural Engineering*, 18(5):056057, 2021.
- Zhang, K., Ye, Z., Ai, Q., Xie, X., and Liu, Y. Gnn4eeg: A benchmark and toolkit for electroencephalography classification with graph neural network. In *Companion of the 2024 on ACM International Joint Conference on Pervasive and Ubiquitous Computing*, pp. 612–617, 2024.
- Zheng, W.-L. and Lu, B.-L. Investigating critical frequency bands and channels for eeg-based emotion recognition with deep neural networks. *IEEE TAMD*, 7(3):162–175, 2015.
- Zhou, Y., Wu, J., Ren, Z., Yao, Z., Lu, W., Peng, K., Zheng, Q., Song, C., Ouyang, W., and Gou, C. Csbrain: A cross-scale spatiotemporal brain foundation model for eeg decoding. *arXiv preprint arXiv:2506.23075*, 2025.
- Zyma, I., Tukaev, S., Seleznov, I., Kiyono, K., Popov, A., Chernykh, M., and Shpenkov, O. Electroencephalograms during mental arithmetic task performance. *Data*, 4(1), 2019.

This appendix provides additional implementation details, analyses, and experiments to support our main findings. The contents are organized as follows:

- Appx. **A** and **B** provides detailed descriptions of the datasets used for fine-tuning, along with our complete experimental settings.
- Appx. **C** presents the detailed experimental data of all 9 models on the 14 benchmark datasets that are not included in the main text due to space limitations.
- Appx. **D** and **E** contains further analysis on the training dynamics and visualizations of the EEG classification behavior.
- Appx. **F** concludes with a discussion of the limitations of the current work and outlines promising directions for future research.

## A. Datasets Description

Detailed information for the evaluation datasets is in Tab. 1:

1. Seizure Detection: Siena (Detti et al., 2020) (binary classification with seizure or healthy);
2. Emotion Recognition: SEED (Zheng & Lu, 2015) (3-class classification with sad, neutral or happy), SEED-V (Liu et al., 2022) (5-class classification with disgust, fear, sad, neutral or happy), SEED-VII (Jiang et al., 2024a) (7-class classification with disgust, fear, sad, neutral, happy, anger or surprise);
3. Motor Imagery: PhysioMI (Schalk et al., 2004) (4-class classification with left fist, right fist, both fists or feet), Mimul-11 (Jeong et al., 2020) (3-class classification with reaching, grasping or twisting), BCIC-2a (Rashid et al., 2020) (4-class classification with left hand, right hand, feet or tongue);
4. Mental Stress: Workload (Zyma et al., 2019) (binary-class classification with arithmetic calculation or resting);
5. Sleep Staging: HMC (Alvarez-Estevez & Rijsman, 2021) (5-class classification with wake, REM, N1, N2 or N3);
6. Anomalous Event Detection: TUEV (Harati et al., 2015) (6-class classification with spike and slow wave, generalized periodic epileptiform discharge, periodic lateralized epileptiform discharge, eye movement artifact or background);
7. Abnormal Classification: TUAB (López et al., 2015) (binary-class classification with abnormal or normal);
8. Visual Target Detection: Things-EEG-2 (Gifford et al., 2022) (binary-class classification with target or non-target);
9. Alzheimer’s Disease Identification: ADFTD (Miltiadous et al., 2023) (3-class classification with Alzheimer’s Disease, Frontotemporal Dementia or healthy);
10. Slowing Event Classification: TUSL (von Weltin et al., 2017) (3-class classification with seizure, slow wave or background).

## B. Experimental Setup

### B.1. Data pre-processing

Our dataset pre-processing pipeline follows a systematic procedure to process EEG data from multiple sources, implemented using MNE-Python (Gramfort et al., 2013). The process begins by resampling the data to a uniform sampling rate based on the pretraining setting of each model, which allows for consistent patch division. To eliminate low-frequency noise, we apply a high-pass Finite Impulse Response (FIR) filter that uses an overlap-add method, a technique chosen for its effectiveness on signals of variable or short durations. Moreover, power-line interference is suppressed using a notch filter at either 50 Hz or 60 Hz; the specific frequency is chosen by manually inspecting each dataset’s power spectrum or its geographical origin. Prior to model input, channels not supported by the model are discarded. The remaining channels from each dataset are then mapped to the standard 10-10 electrode montage based on their names. The data units are then converted from micro-volts ( $\mu V$ ) to Volts to align with the MNE-Python standard. For optimized data management, the

## EEG-FM-Bench

Dataset	Category	#Channel	Duration	#Train	#Valid	#Test	Task
TUAB	Abnormal Classification	23	30	247728	12315	12277	Binary Classification
TUEV	Anomalous Event Detection	21	5	87834	12473	13046	6-class Classification
TUSL	Slowing Event Classification	21,22	10	210	43	37	3-class Classification
SEED	Emotion Recognition	60	10	22455	7875	7560	3-class Classification
SEED-V	Emotion Recognition	60	10	3552	4638	4128	5-class Classification
SEED-VII	Emotion Recognition	60	15	15536	1942	1942	7-class Classification
HMC	Sleep Staging	4	30	91681	22804	22440	5-class Classification
Workload	Mental Stress	19	10	1537	300	297	Binary Classification
Siena	Seizure Detection	29	10	41631	5592	3607	Binary Classification
Mimul-11	Motor Imagery	60	5	31398	5000	4949	3-class Classification
PhysioMI	Motor Imagery	64	4	6210	1734	1803	4-class Classification
BCIC-2a	Motor Imagery	22	4	2784	1152	1152	4-class Classification
Things-EEG-2	Visual Target Detection	63	5	24915	8324	8331	2-class Classification
ADFTD	Alzheimer’s Disease Identification	19	10	4743	1115	1155	3-class Classification

*Table 1.* Detailed information about evaluation datasets.

processed EEG signals are serialized into either the `Parquet` format with `Zstandard` compression for storage efficiency or the `Arrow` format to accelerate data loading and computation. The pipeline also supports large-scale distributed training by accessing datasets directly from remote storage via the `S3` protocol. The entire implementation is built on parallel processing to efficiently handle the terabytes of data in the pre-training corpus.

### B.2. Comparing Foundation Models

Our analysis contrasts seven state-of-the-art EEG Foundation Models: `BENDR` (Kostas et al., 2021), `BIOT` (Yang et al., 2023), `LaBraM` (Jiang et al., 2024b), `EEGPT` (Wang et al., 2024a), `CBraMod` (Wang et al., 2024b), `CSBrain` (Zhou et al., 2025) and `REVE` (Ouahidi et al., 2025). For comparison, we also incorporated two general temporal models `Mantis` (Feofanov et al., 2025) and `Moment` (Goswami et al., 2024). `BENDR` (Kostas et al., 2021) employs a BERT-style objective on a large clinical EEG corpus. To manage data heterogeneity, `BIOT` (Yang et al., 2023) tokenizes different biosignals into a single, sentence-like format. `LaBraM` undergoes pre-training on 2,500 hours of data with `VQ-VAE` (Van Den Oord et al., 2017) modules for dual-domain (frequency/phase) mask learning. `EEGPT` (Wang et al., 2024a) merges dual self-supervised learning with stabilization mechanisms and supports multi-task evaluation by applying different linear probes to its frozen pre-trained backbone. `CBraMod` (Wang et al., 2024b) uses criss-cross attention to capture spatial and temporal features separately in the same transformer layer, which refines its representational ability. `CSBrain` (Zhou et al., 2025) employs cross-scale spatiotemporal tokenization and structured sparse attention to obtain robust EEG representations. `REVE` (Ouahidi et al., 2025) is characterized by the use of the largest pre-training dataset available and 4D Fourier positional encoding, which is paired with an improved MAE reconstruction objective. `Mantis` (Feofanov et al., 2025) and `Moment` (Goswami et al., 2024) are recently proposed, well-performing general-purpose pre-trained models for time series. We include these models in our benchmark as their parameter counts are comparable to current EEG foundation models. Additionally, their high-quality open-source implementations facilitate fair reproduction. In our experiments, we reproduce these models by the benchmark framework on 14 downstream tasks.

### B.3. Evaluation Partition

For most datasets, we partition the data using a subject-level split. In line with common practice, a subject-dependent strategy is adopted for the `SEED`, `SEED-V`, `SEED-VII` datasets to ensure that our metrics are comparable with other baselines. Moreover, we use a greedy, multi-label stratified splitting algorithm to maintain balanced label distributions across the training, validation, and test partitions according to predefined ratios:

- **Siena:** Subject 0-7, 9-13, 16-17 are assigned to the training, validation, test set correspondingly;
- **SEED:** Following prior research, the 15 trials are divided into three sets in a 9:3:3 ratio, and all sessions are merged together thereafter;

- **SEED-V**: Following prior research, the 15 trials are divided into three sets in a 1:1:1 ratio;
- **SEED-VII**: Subjects are randomly split into training, validation, and test sets at a ratio of 8:1:1;
- **PhysioMI**: Subject 1-69,70-88, 89-110 are assigned to the training set, valid set, test set correspondingly;
- **Mimul-11**: Stratified splitting is employed to achieve approximate ratios of 0.76, 0.12, and 0.12 for training, validating, and testing;
- **BCIC-2a**: Subject 1-5,6-7, 8-9 are assigned to the training set, valid set, test set correspondingly;
- **Workload**: Stratified splitting is employed to achieve approximate ratios of 0.72, 0.14, and 0.14 for training, validating, and testing;
- **HMC**: Subjects are randomly split into training, validation, and test sets at a ratio of 103:24:24;
- **TUEV** and **TUSL**: Owing to the highly imbalanced label distribution in these datasets, the stratified splitting function is employed to create three splits from all the data, approximately aligning with predefined ratios of 0.8, 0.1, and 0.1;
- **TUAB**: The validation and test sets are obtained by equally splitting the original evaluation set by subject, while the training set remains unchanged;
- **Things-EEG-2**: Split by subject with predefined ratios of 0.6, 0.2, and 0.2;
- **ADFTD**: Stratified splitting is employed to achieve approximate ratios of 0.70, 0.15, and 0.15 for training, validating, and testing.

#### B.4. Evaluation Metrics

To address the class imbalance in downstream datasets, the following evaluation metrics are adopted for comparison:

- **Balanced Accuracy**: the arithmetic mean of recall (sensitivity) across all classes, mitigating the impact of imbalanced class distributions. It is effective for evaluating classification models on datasets with significant disparities in class proportions, which is formulated as:

$$\text{B-Acc} = \frac{1}{C} \sum_{i=1}^C \frac{TP_i}{TP_i + FN_i}, \quad (6)$$

where  $C$  is the number of classes,  $TP_i$  and  $FN_i$  denote true positives and false negatives for class  $i$ .

- **Weighted F1**: a harmonic mean of precision and recall, weighted by the number of true instances in each class. This metric accounts for class imbalance by assigning higher importance to classes with larger sample sizes, ensuring a more representative evaluation of model effectiveness, which can be formulated as

$$\text{Pre}_i = \frac{TP_i}{TP_i + FP_i}, \quad \text{Rec}_i = \frac{TP_i}{TP_i + FN_i}, \quad (7)$$

$$\text{W-F1} = \sum_{i=1}^C w_i \cdot \frac{2 \cdot \text{Pre}_i \cdot \text{Rec}_i}{\text{Pre}_i + \text{Rec}_i}, \quad (8)$$

where  $FP_i$  denotes false positives for class  $i$ , and  $w_i$  is the weight of class  $i$  based on its support.

- **AUROC**: area under the ROC curve. It reflects the model's ability to discriminate between classes across all possible decision boundaries, which is formulated as

$$\text{TPR} = \frac{TP}{TP + FN}, \quad \text{FPR} = \frac{FP}{FP + TN}, \quad (9)$$

$$\text{AUROC} = \int_0^1 \text{TPR}(f) df, \quad f = \text{FPR}. \quad (10)$$

- **AUC-PR**: area under the precision-recall curve. It provides a holistic evaluation of model performance under class imbalance, which can be formulated as

$$\text{AUC-PR} = \int_0^1 \text{Pre}(r) dr, \quad r = \text{Rec}. \quad (11)$$

- **Cohen’s Kappa**: the agreement level between predicted and true labels by comparing observed and expected frequencies along the diagonal of a confusion matrix. It is particularly suited for multi-class classification scenarios, which can be formulated as

$$\kappa = \frac{p_o - p_e}{1 - p_e}, \quad (12)$$

where  $p_o$  is the observed agreement and  $p_e$  is the expected agreement.

Among these metrics, AUROC and AUC-PR are used to evaluate binary classification tasks, while Cohen’s Kappa and Weighted F1 are applied to multi-category classification. Together, these metrics provide a robust evaluation framework under class imbalance.

### B.5. Training Settings

To facilitate data loading, all samples in the datasets are transformed into an `Arrow` dataset after pre-processing, thus speeding up distributed computing and leveraging the GPU’s direct data access functionality. All experiments are conducted using Python 3.11.13, PyTorch 2.7.1, and CUDA 12.8 on two A800 GPUs. We enable autonomous mixed precision in the `bfloat16` data type to improve GPU memory utilization and introduce `GradScaler` to prevent gradient explosion. We employ the AdamW and a two-phase learning rate scheduler, which combines linear warm-up with cosine annealing. The warm-up learning rate factor is set to 0.1. The total training duration is 30 epochs, including 3 warm-up epochs. The gradient clipping value is 1.0. For EEGPT, we adopt the OneCycle scheduler according to the original paper. To ensure consistency, we adopt the procedure from the REVE paper and apply a freezing warmup epoch for optimal classification head initialization. Weight decay is set to 0.01 except CBraMod for 0.05 to enhance the regularization. Batch size is 128. During downstream fine-tuning, we first set the maximum learning rate following the corresponding open-source implementations. On this basis, we performed a grid search over the learning rate and the hidden dimension of the average-pooling classification head. All experiments were repeated across 5 different random seeds for reliability. We also adopted a differential-learning-rate strategy, configuring the backbone’s learning rate to a fraction (e.g., one-tenth, one-fifth, or one-half) of that assigned to the classifier. The final model for each task is selected based on its validation set performance, with results reported on the held-out test set.

### B.6. Model Configurations

Because several pre-trained architectures were optimized for training with additional information or fixed input montage, they cannot directly accommodate the default setting used in our pipeline. We therefore applied model-specific adaptation strategies:

- **BENDR** and **BIOT**: A dynamic-routing convolutional block was inserted ahead of the backbone. This block employs several `Conv1dwithConstraint` layers that project the input recordings onto the channel configuration expected by the pre-trained weights, thereby harmonizing mismatched channel counts.
- **EEGPT**: As EEGPT already covers almost all electrodes in the ‘EasyCap-M1’ montage provided by MNE, performance loss due to the slightly sparser 10-10 layout is negligible. We thus implemented an Adapter that simply removes the electrodes unsupported by the model.
- **LaBraM** and **CBraMod**: For these models, the original spatial channel layout was flattened into a one-dimensional ordering compatible with their input format.
- **CSBrain**: We aligned the input of all benchmark datasets with the CSBrain’s specification by reordering channels according to their brain region labels, as per its open-source implementation.

- **REVE** relies on a fixed, predefined 4D positional encoding scheme. We load the official released positional encoding checkpoint in the adapter.

These adaptations allow each model to ingest the full breadth of our dataset while preserving compatibility with their pre-trained parameters.

## C. Detailed Results

This section presents the complete quantitative results for the 14 datasets not included in the main text due to space limitations. We analyze performance variations across different fine-tuning strategies (Full-Parameter, Frozen, LoRA), task setups (Single-Task vs. Multi-Task), and classifier head architectures. Tab. 2- 9 compares all 9 models across the benchmark tasks under different fine-tuning strategies. Specifically:

- Tab. 2 reports **full-parameter single-task** fine-tuning results;
- Tab. 3 reports **full-parameter multi-task** fine-tuning results;
- Tab. 4 reports **frozen-backbone multi-task** results;
- Tab. 5 reports **LoRA multi-task** fine-tuning results;
- Tab. 6 **multi-task training from scratch** (randomly initialized backbone) to isolate the benefit of pre-training.
- Tab. 7 and Tab. 8 study the role of **classifier head design** under multi-task fine-tuning;
- Tab. 9 reports the performance of two **general time-series foundation models** (adapted to EEG inputs) to contextualize the advantage of EEG-specific inductive biases.

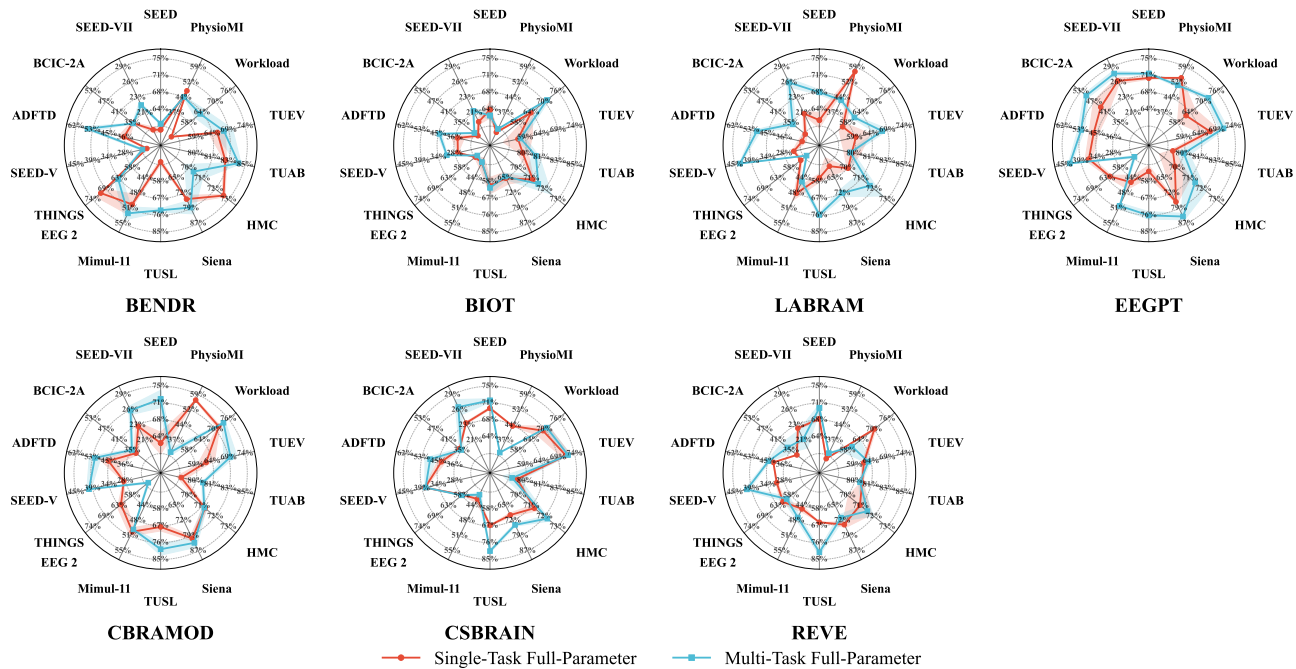


Figure 12. Performance comparison between single-task and multi-task fine-tuning for all 7 EEG-FMs.

### C.1. Key patterns across fine-tuning strategies

**Single-task vs. multi-task.** Comparing Tab. 2 (single-task) and Tab. 3 (multi-task), multi-task learning often acts as a regularizer that mitigates overfitting and improves robustness on several datasets, but can also introduce negative transfer for certain paradigms. This motivates the diagnostic analyses in Appx. D and highlights the need for better multi-task optimization (e.g., task balancing and conflict-aware updates).

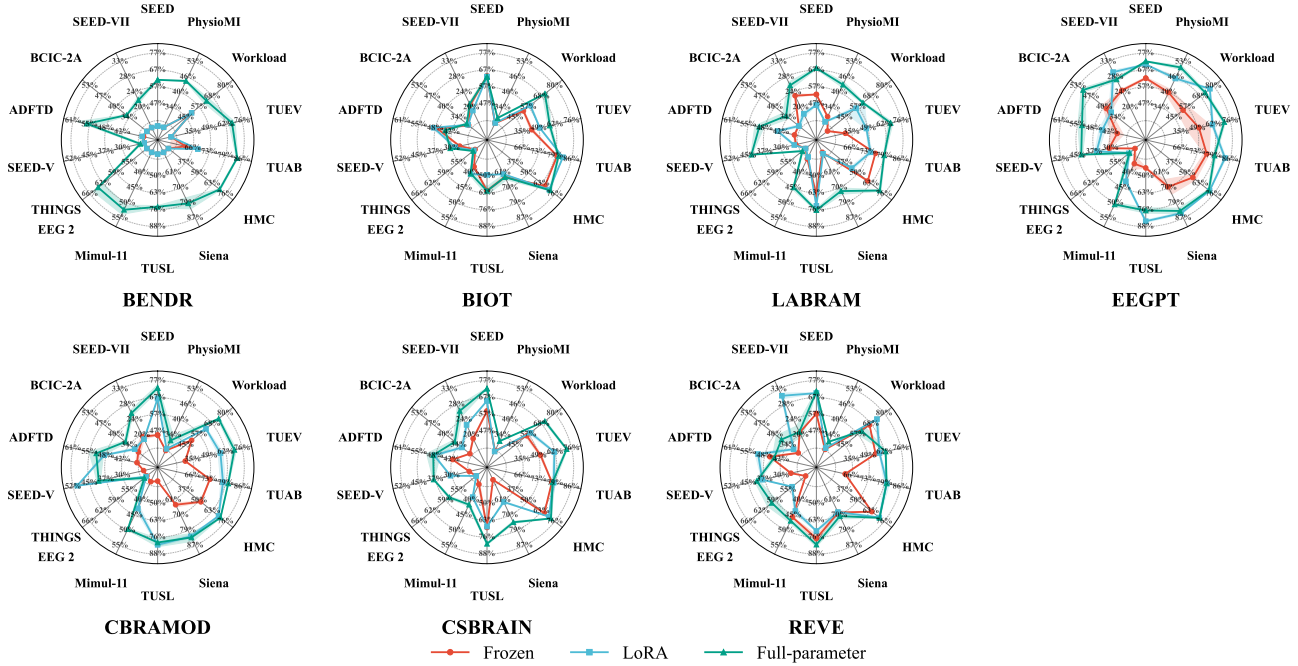


Figure 13. Performance comparison among fine-tuning strategies for all 7 EEG-FMs.

**Frozen backbone vs. LoRA adaptation.** Tab. 4 shows that freezing the backbone can lead to a generalization gap, suggesting that pre-trained representations are not always directly usable without adaptation. Tab. 5 demonstrates that LoRA provides a parameter-efficient alternative that can close part of this gap on many tasks, while still being limited by task conflicts and representation mismatch in hard-transfer settings.

**Fine-tune from checkpoint vs. training from scratch.** Tab. 6 shows that while from-scratch training generally lags behind pre-trained models, the gap is often narrow, and in some cases it even achieves comparable or slightly better results. This suggests that the current pre-training paradigm may not be fully efficient, as the architectural capacity itself can approach similar performance without extensive pre-training.

**C.2. Classifier head ablations**

Tab. 7, 8 show that stronger heads do not uniformly improve performance across paradigms. While high-capacity heads can help in tasks where discriminative evidence is sparse or distributed, they may also exacerbate overfitting when the backbone representation is misaligned with downstream supervision.

**C.3. General time-series foundation models**

Tab. 9 compares EEG-FMs against general time-series foundation models. The performance gap in most EEG paradigms suggests that EEG-specific design choices (e.g., channel handling, spatial-temporal tokenization, and objective alignment) remain important for reliable transfer.

**D. Extended Training Dynamics Analysis**

**D.1. CBraMod**

The results in Fig. 15 and 16 suggest that multi-task training leads to measurable improvements in CBraMod’s representation quality, reflected in higher cosine similarity and subspace affinity. Fig. 18 illustrates that CbraMod’s pre-training objective and fine-tuning objective exhibit a significant conflict in their gradient dynamics, and they primarily affect different model layers. Fig. 19 reveals an interesting divergence: while the intermediate representations from scratch training can rapidly align with the fine-tuned pre-trained model, the underlying gradient energy flow follows a fundamentally different trajectory.

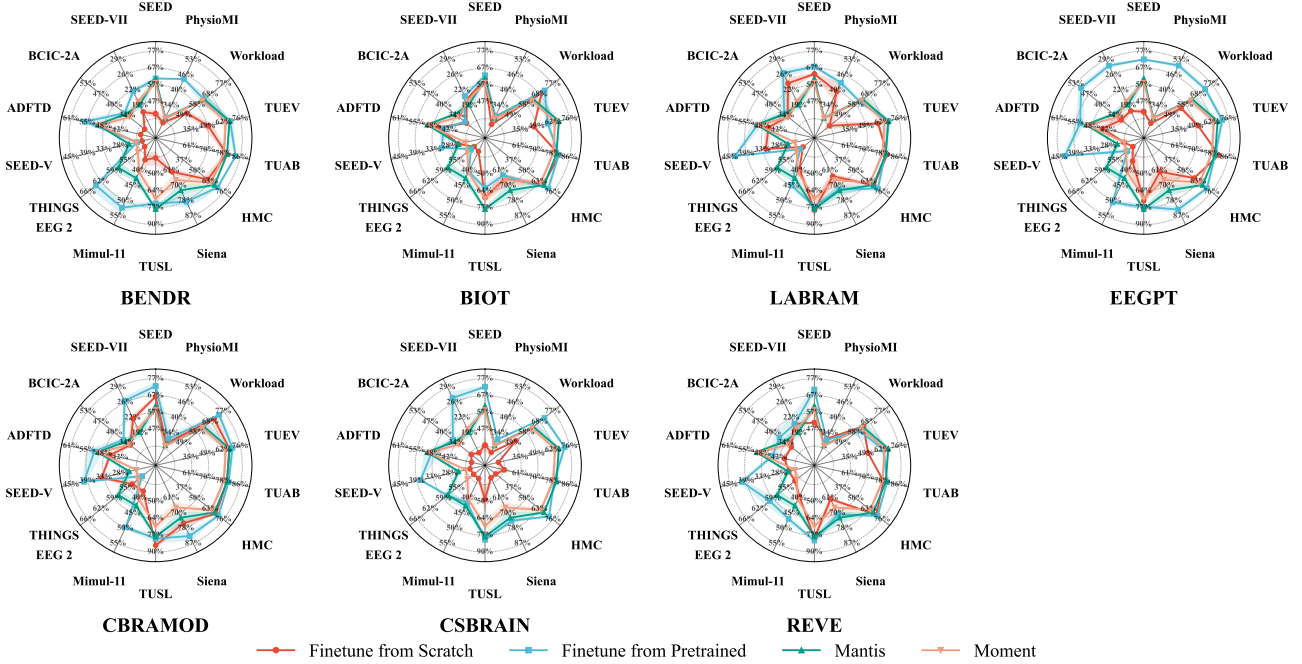


Figure 14. Performance comparison between fine-tuning from scratch and from pre-trained model for all 7 EEG-FMs.

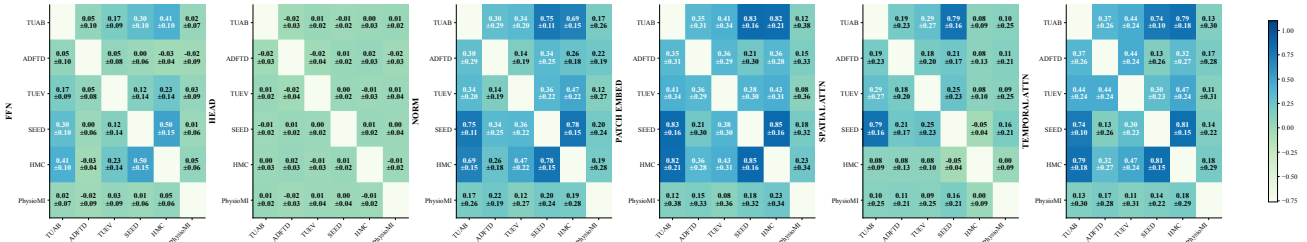


Figure 15. Cross-task gradient cosine similarity correlation analysis for CBraMod.

## D.2. CSBrain

For CSBrain, Fig. 20, 21 provide the cross-task gradient correlation and subspace affinity analyses, respectively. The results in these two figures indicate that the core architecture of CSBrain struggles to achieve performance gains through multi-task training. We hypothesize that the multi-scale modules and brain region attention in CSBrain’s backbone design have difficulty adapting to the rapidly shifting data characteristics during fine-tuning.

Fig. 23 analyzes the gradient alignment between pre-training and downstream tasks. It reveals that CSBrain struggles to effectively optimize its embedding module parameters in both scenarios, and does so in divergent directions, as evidenced by low cosine similarity and high conflict frequency. Fig. 24 indicates that the shallow layers in the CSBrain backbone exhibit markedly different behaviors between the randomly initialized and pre-trained models. Furthermore, modules such as the region attention and feed-forward networks appear particularly resistant to effective optimization if training starts from scratch. Fig. 25 shows that the randomly initialized CSBrain model exhibits abnormally large gradient norms and loss values. Although both metrics drop rapidly during training, we observed in subsequent phases that the model remains prone to collapse when fine-tuned from scratch.

## E. Visualization

To complement the quantitative results, this section provides a qualitative analysis of the feature representations learned by each foundation model. We use t-SNE (Maaten & Hinton, 2008) to visualize the feature embeddings and Integrated

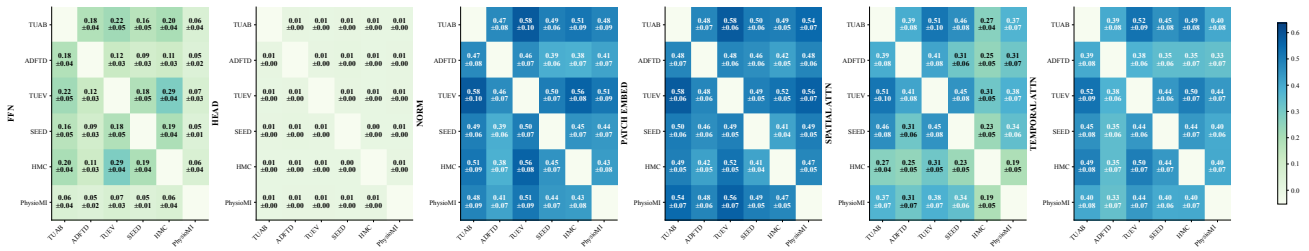


Figure 16. Cross-task subspace affinity analysis for CBraMod.

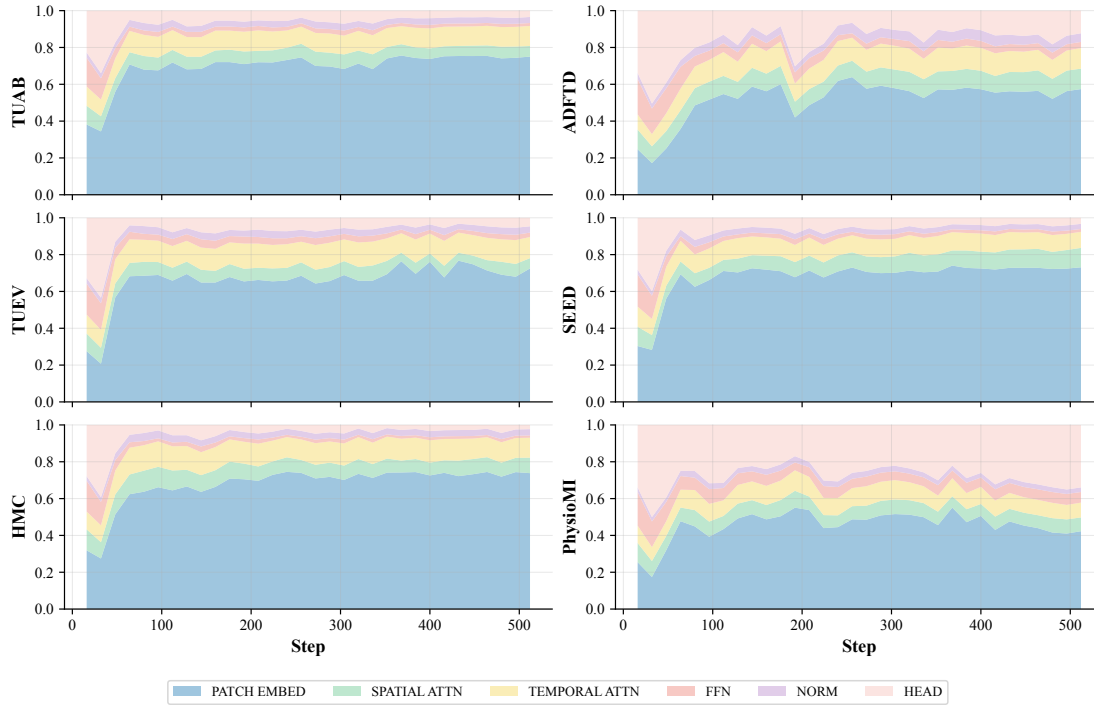


Figure 17. Cross-task evolution dynamics analysis for CBraMod.

Gradients (Sundararajan et al., 2017) to infer the neurophysiological basis for model decisions, focusing on the results from the full-parameter multi-task fine-tuning strategy. Additional visualizations are presented for TUEV, SEED-VII, Mimul-11, ADFTD, and HMC datasets.

- **TUEV**: This 6-class classification task involves identifying various epileptiform discharges and artifacts. The t-SNE plots (Fig. 26) show that CBraMod, EEGPT and CSBrain produce more coherent clusters, aligning with their superior B-Acc scores in the main text. In contrast, the embeddings from BENDR and BIOT are heavily overlapped or same category fail to cluster together, reflecting their lower quantitative performance. The Integrated Gradients maps for the top models indicate a focus on temporal and central channels, which is consistent with the typical scalp distribution of spike-wave discharges.
- **SEED-V**: This 5-class emotion task is notoriously difficult. The visualizations reveal that all models struggle to form well-separated clusters, which corresponds to the low B-Acc scores across the board (Fig. 27). Nonetheless, EEGPT and LaBraM show emergent structures in their embeddings that are absent in other models. The saliency maps suggest that these models attend to channels over the prefrontal and temporal cortices, regions known to be involved in emotion processing, reaffirming the findings from the main text.
- **Mimul-11**: For this 3-class motor imagery task, the t-SNE (Fig. 28) plots for EEGPT and BENDR show the clearest class separation, which is reflected in their higher B-Acc scores relative to other models in the multi-task setting. The

Integrated Gradients visualizations highlight activity in the central and parietal areas of the scalp, corresponding to the location of the motor and somatosensory cortices that govern upper limb movements.

- **ADFTD**: This task requires discriminating between Alzheimer’s Disease (AD), Frontotemporal Dementia (FTD), and healthy controls (CN). The t-SNE (Fig. 29) plots show that BENDR and EEGPT, which performed surprisingly well on this task in the multi-task setting, produces reasonably distinct clusters for the AD and CN classes, though the FTD class remains mixed for BENDR. The saliency maps for the better-performing models indicate a focus on frontal, temporal and parietal channels, which aligns with the known progression of cortical atrophy in Alzheimer’s Disease.
- **HMC**: For this 5-class sleep staging task, the t-SNE visualizations (Fig. 30) show that the clusters of EEGPT appear highly fragmented, while CBraMod’s visualization exhibits a radial pattern where the central N2 category overlaps excessively with other categories, which indicates the suboptimal metrics in the table of main text.

## F. Limitations and Summary

### F.1. Limitations

**Scope of Benchmark** While EEG-FM-Bench covers a diverse set of datasets and paradigms, it cannot represent the full spectrum of EEG applications (e.g., multi-modal EEG settings, closed-source proprietary models, and certain clinical workflows). Future iterations can expand the suite of tasks and continuously integrate new state-of-the-art models to ensure the benchmark remains relevant.

**Negative transfer in multi-task learning.** Multi-task fine-tuning can improve generalization but also risks negative transfer when datasets have conflicting objectives or incompatible inductive biases. Our current implementation uses a unified optimizer and learning strategy for all tasks, which may be suboptimal for managing gradient conflicts. Conflict-aware updates, adaptive task weighting, or modular/shared-private designs are promising directions.

**Rapid evolution of EEG foundation models.** EEG-FMs are evolving quickly in architecture, pre-training objectives, and data scale. This creates a moving target for fair comparison and emphasizes the need for open, reproducible, and continuously maintainable benchmarking infrastructure.

### F.2. Summary

This appendix provides supplementary details that support the main paper, including:

- Dataset-level descriptions and experimental specifics;
- Detailed training settings;
- Complete quantitative performance tables under multiple fine-tuning strategies and classifier heads;
- Qualitative visualizations and diagnostic analyses that help interpret generalization and optimization behavior

Together with the main paper, these results provide standardized baselines and mechanistic insights to guide future EEG-FM development, with an emphasis on benchmarking unity, pre-training efficiency, and robust multi-task transfer.

Table 2. Performance comparison of 7 EEG-FMs on 14 BCI tasks under **full-parameter single-task** fine-tuning with **average pooling** classification head.

Dataset	Metrics	BENDR	BIOT	LaBraM	EEGPT	CBraMod	CsBrain	REVE
SEED	B-Acc	59.50±00.42	63.87±01.77	61.59±01.71	70.83±00.28	62.59±02.40	70.23±00.25	67.90±00.37
	F1/AUROC	58.88±00.98	63.12±01.94	60.30±01.60	70.48±00.16	61.67±02.66	70.70±00.22	67.20±00.49
	Kappa/AUCPR	39.42±00.64	45.99±02.67	43.28±02.48	56.41±00.42	44.36±03.58	55.70±00.28	52.03±00.62
PhysioMI	B-Acc	47.78±00.28	27.38±00.35	57.27±00.26	54.16±00.18	56.74±00.36	43.97±00.12	27.90±00.28
	F1/AUROC	42.72±08.93	26.01±00.62	57.29±00.25	53.27±00.92	56.74±00.39	43.87±00.12	27.33±00.48
	Kappa/AUCPR	36.48±08.47	03.18±00.46	43.00±00.35	38.04±01.08	42.31±00.48	25.27±00.21	03.87±00.38
Workload	B-Acc	50.00±00.00	63.98±00.66	55.82±01.72	62.31±03.98	71.94±00.60	69.53±02.65	70.50±00.99
	F1/AUROC	52.36±01.25	77.68±01.62	78.19±00.48	70.46±04.00	81.63±01.63	77.07±04.26	78.53±00.56
	Kappa/AUCPR	30.70±00.55	69.30±02.27	59.36±01.26	48.13±06.90	59.73±01.79	64.67±03.20	64.43±00.39
TUEV	B-Acc	65.53±02.40	57.07±04.29	59.58±04.31	66.86±02.54	62.22±02.49	71.20±01.34	61.93±00.54
	F1/AUROC	80.95±02.18	74.34±04.00	77.72±03.25	83.95±00.14	76.78±02.10	85.07±00.85	81.23±00.92
	Kappa/AUCPR	66.62±04.07	39.55±04.15	64.06±05.03	74.45±00.09	61.42±02.74	74.67±01.44	68.33±01.55
TUAB	B-Acc	82.72±00.12	79.52±00.59	79.50±00.81	78.66±00.24	78.31±00.46	78.97±00.17	80.53±00.12
	F1/AUROC	89.52±00.14	88.27±00.16	86.91±00.51	87.52±01.01	88.02±01.08	85.33±01.51	87.43±01.04
	Kappa/AUCPR	90.68±00.13	88.45±00.07	83.86±01.96	86.94±02.15	88.24±01.09	82.73±04.69	86.00±02.20
HMC	B-Acc	72.63±00.13	71.01±00.07	69.87±00.10	69.67±01.24	71.14±00.14	71.13±00.26	70.83±00.94
	F1/AUROC	73.67±00.53	72.27±00.11	70.92±00.23	73.03±00.32	72.76±00.55	73.10±00.22	73.33±00.90
	Kappa/AUCPR	65.86±00.70	64.40±00.35	63.10±00.31	64.64±00.92	64.86±00.41	65.20±00.29	64.37±01.39
Siena	B-Acc	74.93±01.76	64.93±02.70	59.11±04.05	76.25±01.02	80.64±01.40	69.37±00.86	74.00±01.36
	F1/AUROC	90.90±03.60	70.17±02.73	81.76±01.97	92.08±01.15	93.86±00.25	78.60±03.34	89.27±02.85
	Kappa/AUCPR	99.81±00.08	98.93±00.20	99.65±00.07	99.81±00.02	99.87±00.01	99.60±00.08	99.77±00.09
TUSL	B-Acc	47.22±01.48	60.05±04.47	55.89±02.31	52.35±03.20	67.53±02.16	66.67±00.21	65.00±00.00
	F1/AUROC	34.17±02.80	56.83±04.49	39.50±01.73	72.68±02.34	64.36±02.66	60.90±02.34	58.70±00.00
	Kappa/AUCPR	17.88±01.95	37.52±06.77	24.71±03.27	66.57±02.63	46.74±03.54	43.63±01.08	40.50±00.00
Mimul-11	B-Acc	50.44±02.30	40.55±01.14	47.80±01.68	45.19±01.69	50.39±01.02	42.67±00.77	45.00±00.62
	F1/AUROC	59.09±01.23	49.68±01.29	57.43±01.27	54.66±01.38	59.86±00.92	51.93±00.87	54.63±00.71
	Kappa/AUCPR	36.10±03.49	14.45±02.10	30.71±03.14	23.68±02.30	36.81±02.73	18.13±02.05	23.10±01.31
Things EEG 2	B-Acc	71.09±02.02	51.70±00.33	53.38±00.39	62.08±00.58	62.40±01.56	57.20±00.29	61.03±00.90
	F1/AUROC	83.09±00.69	66.01±01.00	56.38±01.08	75.69±01.02	77.61±00.32	62.67±00.53	66.77±00.52
	Kappa/AUCPR	52.68±00.45	18.71±00.36	13.65±00.45	33.32±01.46	37.48±00.78	21.53±00.42	22.87±01.72
SEED-V	B-Acc	20.20±00.13	26.66±00.13	24.35±00.55	36.43±01.33	28.34±00.17	38.23±00.24	30.37±00.31
	F1/AUROC	10.72±01.57	25.85±00.13	23.64±01.21	33.00±01.94	27.48±00.89	39.07±00.34	30.60±00.57
	Kappa/AUCPR	00.21±00.13	09.53±00.08	05.61±01.13	18.52±00.67	10.55±00.20	22.70±00.29	12.90±00.64
ADFTD	B-Acc	37.16±02.62	34.95±03.17	27.25±01.98	46.50±02.28	45.02±04.88	43.20±01.93	41.90±00.08
	F1/AUROC	40.38±01.69	36.82±03.14	28.34±02.05	48.77±02.56	44.20±07.00	40.00±03.02	45.87±00.48
	Kappa/AUCPR	07.27±04.67	03.75±03.97	14.31±01.76	21.81±03.72	18.50±07.76	12.27±02.32	16.40±00.08
BCIC-2a	B-Acc	35.21±00.54	28.11±00.60	29.03±00.82	44.07±03.27	33.71±00.86	36.23±00.25	32.73±00.19
	F1/AUROC	33.25±00.57	20.86±00.74	28.50±01.50	38.61±04.23	28.99±01.35	27.03±00.62	31.60±00.16
	Kappa/AUCPR	13.62±00.72	04.07±00.90	05.07±00.68	25.42±04.36	11.61±01.14	15.00±00.33	10.33±00.19
SEED-VII	B-Acc	17.43±00.60	18.89±00.43	20.39±00.41	26.42±00.55	23.10±00.93	23.73±00.17	22.77±00.17
	F1/AUROC	14.20±00.79	16.84±01.12	19.55±03.82	23.89±01.29	21.82±02.00	23.43±00.12	23.67±00.09
	Kappa/AUCPR	03.98±00.69	05.80±00.48	09.42±02.64	14.05±00.99	09.70±02.62	10.40±00.22	10.60±00.08

Table 3. Performance comparison of 7 EEG-FMs on 14 BCI tasks under **full-parameter multi-task fine-tuning with average pooling** classification head.

Dataset	Metrics	BENDR	BIOT	LaBraM	EEGPT	CBraMod	CSBrain	REVE
SEED	B-Acc	60.82±00.19	62.62±00.94	67.71±00.55	71.80±00.17	72.25±01.90	71.92±00.39	70.29±00.78
	F1/AUROC	60.84±00.20	62.57±00.87	68.11±00.66	71.26±00.42	72.90±01.63	71.84±00.20	69.62±00.72
	Kappa/AUCPR	41.59±00.16	44.11±01.42	52.22±00.83	57.86±00.26	58.68±02.91	58.02±00.59	55.59±01.18
PhysioMI	B-Acc	44.77±00.31	29.04±00.24	43.19±01.03	50.52±00.80	31.15±02.27	30.90±00.08	30.63±00.06
	F1/AUROC	44.63±00.03	28.81±00.29	42.38±01.15	50.26±00.76	28.83±03.48	29.84±00.31	29.23±00.91
	Kappa/AUCPR	26.33±00.40	05.39±00.32	24.25±01.37	34.00±01.06	08.21±03.03	07.87±00.10	07.50±00.07
Workload	B-Acc	63.32±02.29	71.37±02.19	61.24±00.64	72.66±00.90	74.12±00.79	71.27±00.75	60.22±03.62
	F1/AUROC	74.09±01.04	72.43±01.94	67.84±04.38	81.16±03.42	83.89±00.93	79.63±01.20	69.60±01.73
	Kappa/AUCPR	54.78±01.84	69.52±00.23	54.94±03.49	64.30±06.48	72.58±01.55	55.10±02.21	62.04±02.41
TUEV	B-Acc	67.46±02.59	57.81±01.30	67.34±02.06	70.85±01.16	69.41±01.86	71.82±00.69	63.24±00.73
	F1/AUROC	84.56±01.82	76.77±00.42	83.14±03.12	86.35±00.47	83.44±00.31	87.00±00.64	84.97±00.33
	Kappa/AUCPR	72.85±02.87	63.24±00.57	72.47±05.02	77.69±01.06	72.02±00.65	77.84±01.55	75.12±00.76
TUAB	B-Acc	84.05±00.26	80.85±00.36	79.36±00.31	79.76±00.59	80.49±00.11	78.46±00.87	80.32±00.17
	F1/AUROC	90.38±00.27	88.67±00.62	85.81±00.94	88.48±00.18	90.18±00.48	84.95±01.23	86.61±01.24
	Kappa/AUCPR	91.58±00.15	89.01±00.47	83.83±01.78	88.18±00.38	90.03±00.55	85.81±01.23	84.56±01.91
HMC	B-Acc	70.21±00.72	71.45±01.05	71.63±01.04	71.30±00.91	71.08±00.15	72.18±00.24	71.43±00.49
	F1/AUROC	72.44±00.65	72.89±00.34	72.28±01.08	72.46±00.96	69.66±00.48	74.16±00.27	74.03±00.46
	Kappa/AUCPR	64.57±00.90	64.89±00.71	65.22±01.23	64.86±00.77	42.73±25.88	66.43±00.16	65.56±01.08
Siena	B-Acc	78.96±03.08	64.07±01.56	71.99±01.78	83.28±01.56	82.75±02.10	74.11±00.60	70.65±01.52
	F1/AUROC	91.31±04.74	78.06±07.16	87.09±03.70	93.44±00.12	92.03±01.90	89.07±02.39	83.56±01.28
	Kappa/AUCPR	99.81±00.11	99.26±00.39	99.76±00.08	99.86±00.00	99.83±00.04	99.72±00.11	99.64±00.03
TUSL	B-Acc	73.35±00.98	61.24±03.28	75.86±01.15	76.12±02.05	79.56±03.24	80.56±00.91	81.20±01.70
	F1/AUROC	70.90±01.73	57.16±05.59	72.74±01.33	84.19±01.04	76.24±04.45	76.72±00.38	77.82±01.29
	Kappa/AUCPR	56.65±02.55	36.19±06.81	59.60±01.81	84.30±01.27	64.72±05.96	65.57±00.41	66.89±02.18
Mimul-11	B-Acc	52.55±01.52	40.43±00.63	45.05±00.66	50.77±00.61	49.87±00.26	41.64±00.54	47.05±00.62
	F1/AUROC	59.61±02.80	49.02±00.73	53.42±01.98	57.44±01.11	48.90±01.52	50.70±00.61	52.82±01.64
	Kappa/AUCPR	38.35±04.93	14.63±01.88	22.60±02.20	31.16±02.43	17.95±00.88	15.94±01.33	20.88±01.87
Things EEG 2	B-Acc	63.62±01.38	50.86±00.25	50.90±00.28	51.54±00.76	50.70±00.68	57.49±00.27	59.43±01.20
	F1/AUROC	77.23±00.88	63.01±03.12	54.16±04.06	66.64±00.04	66.79±02.55	62.47±01.27	69.00±00.53
	Kappa/AUCPR	42.29±01.75	16.11±02.22	13.33±01.32	20.30±00.65	19.49±02.43	19.66±01.93	28.94±00.79
SEED-V	B-Acc	21.75±00.66	30.54±00.18	43.26±00.29	43.07±00.60	40.56±00.77	38.02±00.23	40.84±00.98
	F1/AUROC	19.94±02.58	30.97±00.26	43.20±00.81	42.99±00.54	41.72±00.72	38.07±01.03	40.58±02.00
	Kappa/AUCPR	02.90±00.68	14.14±00.21	28.93±00.50	28.62±00.86	26.22±00.97	22.48±00.42	25.59±01.48
ADFTD	B-Acc	55.71±03.76	44.25±01.34	50.27±01.74	52.91±01.57	51.95±02.84	48.96±02.65	44.38±00.75
	F1/AUROC	56.97±02.75	47.02±01.38	26.17±03.15	54.82±01.30	54.41±03.13	50.17±03.76	50.55±00.43
	Kappa/AUCPR	33.98±04.63	18.77±01.80	52.36±02.23	31.14±01.85	30.06±04.35	24.96±04.13	23.17±00.83
BCIC-2a	B-Acc	34.98±00.25	29.66±00.39	34.58±01.64	50.52±00.93	35.50±00.58	35.50±00.86	36.89±02.52
	F1/AUROC	30.01±02.27	23.61±04.64	31.24±02.71	48.40±01.86	23.97±00.25	27.97±02.36	33.50±00.21
	Kappa/AUCPR	13.31±00.33	05.99±00.45	12.60±02.00	32.37±02.50	14.00±00.77	14.00±01.15	15.86±03.36
SEED-VII	B-Acc	21.98±00.66	20.91±00.41	26.13±00.92	27.78±00.47	26.05±00.72	26.67±01.37	20.76±01.64
	F1/AUROC	19.31±00.87	19.67±01.46	24.74±00.57	25.40±00.12	25.74±01.22	22.68±02.69	19.86±02.08
	Kappa/AUCPR	09.49±01.03	08.46±00.55	13.07±00.93	15.80±01.12	13.09±00.86	11.40±02.04	09.43±00.93

Table 4. Performance comparison of 7 EEG-FMs on 14 BCI tasks under **freezing-parameter multi-task** fine-tuning with **average pooling** classification head.

Dataset	Metrics	BENDR	BIOT	LaBraM	EEGPT	CBraMod	CSBrain	REVE
SEED	B-Acc	33.30±00.00	63.10±00.22	52.13±00.05	61.80±00.65	44.32±00.28	58.57±00.05	57.03±00.05
	F1/AUROC	17.00±00.00	63.07±00.25	51.23±00.34	60.41±01.07	44.50±00.30	58.53±00.05	56.80±00.14
	Kappa/AUCPR	00.00±00.00	44.77±00.33	28.33±00.12	42.89±00.97	16.76±00.45	38.00±00.14	35.63±00.05
PhysioMI	B-Acc	25.00±00.00	26.80±00.33	29.63±00.34	39.90±01.39	26.90±00.24	26.80±00.29	27.37±00.41
	F1/AUROC	10.03±00.05	25.90±00.43	28.97±00.77	39.51±01.92	22.76±00.17	24.77±01.25	26.67±00.76
	Kappa/AUCPR	00.00±00.00	02.40±00.41	06.23±00.42	19.87±01.84	02.54±00.32	02.40±00.37	03.17±00.49
Workload	B-Acc	50.00±00.00	52.17±00.52	29.63±00.34	52.98±04.22	50.00±00.00	55.07±00.94	67.10±00.00
	F1/AUROC	48.83±01.68	83.60±01.96	28.97±00.77	75.19±00.79	66.87±00.17	76.83±00.12	79.83±00.17
	Kappa/AUCPR	24.83±00.87	60.40±01.53	06.23±00.42	49.23±00.69	42.70±00.07	54.73±00.12	61.20±00.85
TUEV	B-Acc	16.70±00.00	42.73±01.11	29.63±00.34	49.83±09.60	28.51±00.45	50.07±01.00	54.83±00.05
	F1/AUROC	44.10±00.00	67.47±00.57	28.97±00.77	75.99±05.48	61.35±00.46	83.00±00.62	72.97±00.12
	Kappa/AUCPR	00.00±00.00	51.00±00.57	06.23±00.42	62.22±09.38	33.37±01.08	71.50±01.40	59.10±00.22
TUAB	B-Acc	63.53±05.85	80.30±00.22	75.87±00.05	76.64±01.04	73.15±00.19	78.20±00.00	63.80±00.08
	F1/AUROC	73.17±00.82	87.50±00.14	84.07±00.05	87.43±00.33	80.41±00.02	87.00±00.08	65.33±00.09
	Kappa/AUCPR	65.93±00.45	87.27±00.57	84.60±00.08	87.47±00.74	79.79±00.15	87.23±00.12	56.27±00.05
HMC	B-Acc	20.00±00.00	66.13±00.21	59.80±00.00	55.61±02.81	51.81±00.55	65.60±00.00	63.80±00.08
	F1/AUROC	20.30±00.00	70.27±00.29	64.10±00.37	56.49±01.41	58.11±00.82	69.73±00.21	65.33±00.09
	Kappa/AUCPR	00.00±00.00	61.03±00.17	53.40±00.16	46.36±02.48	44.95±00.68	62.00±00.28	56.27±00.05
Siena	B-Acc	50.00±00.00	64.03±00.54	50.00±00.00	69.58±04.12	64.17±01.18	50.00±00.00	68.60±00.08
	F1/AUROC	61.20±04.16	75.97±01.93	79.20±02.00	92.20±01.98	90.16±00.41	56.53±12.17	77.87±00.37
	Kappa/AUCPR	99.27±00.12	99.20±00.08	99.53±00.05	99.84±00.03	99.68±00.02	98.10±00.62	99.27±00.05
TUSL	B-Acc	33.30±00.00	61.13±01.20	63.90±02.52	43.81±00.14	33.00±00.00	68.17±01.04	76.57±02.88
	F1/AUROC	17.50±00.00	58.30±01.80	54.57±02.18	67.86±00.00	09.35±01.20	62.93±01.79	71.97±03.70
	Kappa/AUCPR	00.00±00.00	35.43±01.94	37.63±04.29	60.48±02.18	00.00±00.00	47.63±01.93	58.87±04.96
Mimul-11	B-Acc	33.30±00.00	38.13±00.24	35.50±00.43	37.11±01.97	33.95±00.11	34.80±00.59	45.83±00.12
	F1/AUROC	37.90±00.00	47.10±00.16	42.97±00.88	44.95±03.07	40.09±00.18	42.73±01.05	54.87±00.05
	Kappa/AUCPR	00.00±00.00	09.00±00.22	04.60±00.93	10.06±03.66	01.51±00.25	03.10±01.39	23.00±00.24
Things EEG 2	B-Acc	50.00±00.00	50.33±00.05	50.00±00.00	50.00±00.00	50.00±00.00	50.00±00.00	50.00±00.00
	F1/AUROC	51.17±01.46	65.00±00.70	53.77±00.45	59.57±00.42	53.85±00.07	51.63±02.31	53.17±01.46
	Kappa/AUCPR	11.23±00.39	19.57±00.19	12.57±00.17	14.18±00.15	12.29±00.13	12.10±00.94	12.10±00.73
SEED-V	B-Acc	20.00±00.00	26.27±00.47	23.23±00.48	30.48±00.73	20.28±00.02	21.97±00.12	25.43±00.33
	F1/AUROC	06.00±01.98	24.77±00.90	19.63±00.91	28.71±01.45	10.93±00.03	14.43±00.62	24.07±00.41
	Kappa/AUCPR	00.00±00.00	09.17±00.54	04.43±00.68	12.90±00.57	00.45±00.03	02.50±00.16	07.07±00.37
ADFTD	B-Acc	33.30±00.00	47.37±00.09	36.43±00.41	39.03±02.48	35.92±00.27	41.30±00.28	46.10±00.24
	F1/AUROC	22.17±00.75	50.47±00.05	38.47±00.70	32.02±00.53	34.16±01.32	42.23±00.25	49.70±00.14
	Kappa/AUCPR	00.00±00.00	23.47±00.21	06.90±01.14	07.72±03.37	05.26±00.29	12.40±00.45	23.20±00.29
BCIC-2a	B-Acc	25.00±00.00	28.73±00.54	28.40±00.24	39.06±02.09	29.17±01.03	28.13±00.17	28.63±00.45
	F1/AUROC	10.00±00.00	20.00±00.43	22.83±00.45	33.59±02.00	24.94±01.72	18.57±00.12	18.17±01.40
	Kappa/AUCPR	00.00±00.00	04.97±00.79	04.57±00.33	18.75±02.79	05.56±01.37	04.17±00.26	04.90±00.57
SEED-VII	B-Acc	14.30±00.00	20.60±00.45	23.23±00.48	24.72±00.32	19.43±00.72	18.90±00.29	20.57±00.17
	F1/AUROC	03.63±00.61	16.60±00.43	19.63±00.91	21.85±02.00	16.76±00.29	16.60±00.50	20.50±00.33
	Kappa/AUCPR	00.00±00.00	07.50±00.42	04.43±00.68	13.35±00.35	06.97±00.95	06.27±00.41	08.50±00.29

Table 5. Performance comparison of 7 EEG-FMs on 14 BCI tasks under LoRA multi-task fine-tuning with average pooling classification head.

Dataset	Metrics	BENDR	BIOT	LaBraM	EEGPT	CBraMod	CSBrain	REVE
SEED	B-Acc	33.30±00.00	62.70±00.14	45.90±00.22	69.97±00.05	66.07±00.21	64.67±00.05	69.23±00.21
	F1/AUROC	17.00±00.00	62.60±00.08	43.07±02.04	69.27±00.61	65.57±00.38	64.07±00.17	68.97±00.46
	Kappa/AUCPR	00.00±00.00	44.20±00.22	18.90±00.29	55.10±00.08	49.27±00.29	47.20±00.08	54.03±00.34
PhysioMI	B-Acc	25.10±00.08	26.93±00.05	27.40±00.16	45.83±00.85	27.60±00.22	26.47±00.31	27.93±00.05
	F1/AUROC	11.90±02.55	26.17±00.48	20.47±01.13	45.33±00.74	24.50±02.03	24.73±01.05	26.90±00.45
	Kappa/AUCPR	00.13±00.12	02.57±00.09	03.20±00.24	27.80±01.10	03.50±00.29	01.97±00.45	03.90±00.08
Workload	B-Acc	50.00±00.00	58.30±00.71	55.10±07.21	76.87±00.37	62.80±00.57	58.43±01.27	73.70±01.65
	F1/AUROC	49.20±00.64	78.83±00.58	72.07±02.26	87.63±01.09	81.63±00.90	82.37±02.53	85.27±00.48
	Kappa/AUCPR	25.47±01.06	58.60±00.57	43.80±03.72	76.43±01.52	62.80±01.93	64.50±02.19	65.73±01.25
TUEV	B-Acc	16.70±00.00	49.47±00.33	47.13±00.59	61.07±00.98	57.80±02.06	61.57±00.68	58.07±00.29
	F1/AUROC	44.10±00.00	72.03±00.29	72.33±01.32	86.83±00.24	77.60±03.19	78.97±01.11	75.47±02.05
	Kappa/AUCPR	00.00±00.00	53.53±00.50	54.33±02.28	79.60±01.07	63.07±04.76	63.70±01.63	61.20±02.87
TUAB	B-Acc	68.37±00.12	82.60±00.00	73.93±00.65	83.93±00.50	78.40±00.93	78.97±00.71	80.43±01.04
	F1/AUROC	76.77±00.21	89.57±00.21	82.57±00.48	91.93±00.39	86.07±00.97	87.07±01.01	88.03±00.54
	Kappa/AUCPR	71.93±00.41	90.60±00.16	81.67±00.74	91.93±00.21	87.07±00.95	87.23±01.09	88.07±01.16
HMC	B-Acc	20.00±00.00	70.43±00.19	44.10±01.31	71.97±00.12	69.13±00.17	69.93±00.09	71.03±00.25
	F1/AUROC	20.30±00.00	74.03±00.19	47.10±01.56	72.27±00.39	71.60±00.73	73.13±00.17	71.77±00.25
	Kappa/AUCPR	00.00±00.00	65.90±00.24	32.67±01.39	64.63±00.21	63.00±00.28	64.70±00.14	63.83±00.26
Siena	B-Acc	50.00±00.00	62.40±00.00	50.80±00.57	84.57±00.61	82.13±00.78	62.57±00.52	68.33±01.46
	F1/AUROC	80.70±05.21	83.87±02.68	68.57±17.66	94.50±00.45	93.20±01.35	84.43±02.09	88.73±01.05
	Kappa/AUCPR	99.67±00.19	99.53±00.09	99.20±00.65	99.90±00.00	99.83±00.05	99.73±00.05	99.83±00.05
TUSL	B-Acc	33.30±00.00	49.07±00.24	72.60±02.48	84.27±00.94	81.33±01.04	67.50±00.00	70.83±00.45
	F1/AUROC	25.70±00.00	49.13±00.17	67.17±02.78	83.00±00.00	78.27±01.37	61.83±00.24	68.30±00.08
	Kappa/AUCPR	00.00±00.00	19.00±00.37	52.77±03.84	73.90±00.14	67.20±01.98	45.93±00.24	52.67±00.26
Mimul-11	B-Acc	33.30±00.00	40.57±00.37	34.87±00.24	43.00±00.36	42.90±00.92	39.10±00.24	43.77±00.82
	F1/AUROC	37.90±00.00	49.53±00.31	41.67±00.45	52.00±00.50	50.00±01.22	48.23±00.26	50.33±01.98
	Kappa/AUCPR	00.00±00.00	12.40±00.57	03.63±00.40	18.90±00.29	15.07±01.62	12.13±00.37	17.90±02.01
Things EEG 2	B-Acc	50.00±00.00	50.67±00.05	50.00±00.00	51.70±00.37	50.23±00.05	50.00±00.00	53.77±00.12
	F1/AUROC	50.27±00.12	64.13±00.17	55.27±02.33	61.83±00.21	57.60±00.79	54.43±00.62	60.70±00.24
	Kappa/AUCPR	11.03±00.05	19.47±00.05	13.13±01.13	14.97±00.31	14.17±00.31	13.03±00.21	15.70±00.22
SEED-V	B-Acc	20.00±00.00	28.37±00.12	23.93±00.53	36.07±00.85	50.23±00.05	30.43±00.17	38.37±00.21
	F1/AUROC	08.80±00.00	27.87±00.33	22.10±00.80	35.77±01.77	57.60±00.79	28.20±00.65	38.87±00.42
	Kappa/AUCPR	00.00±00.00	11.33±00.19	05.17±00.69	20.10±00.75	14.17±00.31	13.17±00.29	22.70±00.49
ADFTD	B-Acc	33.87±00.80	48.77±01.40	43.07±00.66	44.93±01.18	48.83±00.50	48.60±00.45	50.73±01.28
	F1/AUROC	18.77±07.78	51.33±01.88	45.77±00.76	45.80±01.31	51.57±00.25	47.20±00.57	24.73±02.80
	Kappa/AUCPR	00.83±01.18	25.27±01.93	18.40±01.28	17.73±01.70	26.27±01.86	27.33±00.74	56.03±00.40
BCIC-2a	B-Acc	25.00±00.00	29.00±00.14	28.30±00.73	36.70±01.15	31.00±00.70	32.00±00.99	30.90±00.78
	F1/AUROC	10.00±00.00	19.40±00.14	17.87±01.01	32.67±03.16	22.20±02.19	20.77±01.11	22.47±01.35
	Kappa/AUCPR	00.00±00.00	05.33±00.19	04.43±00.93	15.60±01.53	08.03±00.98	09.30±01.35	07.87±00.98
SEED-VII	B-Acc	14.30±00.00	19.07±00.17	18.13±00.71	29.83±00.53	18.73±00.19	22.73±00.09	30.90±00.78
	F1/AUROC	04.77±00.33	15.73±00.48	13.30±01.36	27.30±01.55	14.87±01.00	22.27±00.24	22.47±01.35
	Kappa/AUCPR	00.00±00.00	06.50±00.28	04.37±01.23	17.73±01.03	05.00±00.36	10.80±00.08	07.87±00.98

Table 6. Performance comparison of 7 EEG-FMs on 14 BCI tasks under **full-parameter multi-task** fine-tuning from **randomly initialized** model with **average pooling** classification head.

Dataset	Metrics	BENDR	BIOT	LaBraM	EEGPT	CBraMod	CSBrain	REVE
SEED	B-Acc	40.50±01.92	60.40±00.29	63.43±00.62	41.70±01.88	66.27±00.21	38.20±03.67	51.27±00.31
	F1/AUROC	37.07±02.82	60.53±00.26	63.20±00.51	41.53±02.30	64.97±00.47	30.77±04.46	50.50±00.33
	Kappa/AUCPR	10.73±02.88	40.73±00.46	45.33±01.00	12.83±03.06	49.57±00.29	07.30±05.49	27.03±00.47
PhysioMI	B-Acc	26.37±01.24	25.57±00.09	39.53±03.19	26.10±00.36	29.30±00.83	25.37±00.12	31.23±00.12
	F1/AUROC	13.97±02.43	18.33±01.45	38.93±04.42	22.93±02.14	28.73±00.97	17.97±01.05	30.93±00.17
	Kappa/AUCPR	01.80±01.69	00.77±00.09	19.47±04.27	01.43±00.45	05.73±01.16	00.47±00.21	08.37±00.17
Workload	B-Acc	50.97±01.37	69.30±00.73	39.53±03.19	55.40±00.96	70.53±02.00	50.73±00.77	63.90±00.45
	F1/AUROC	46.67±05.48	85.43±00.61	38.93±04.42	67.93±02.69	77.17±02.44	58.13±03.42	68.07±01.37
	Kappa/AUCPR	25.73±04.25	64.17±00.96	19.47±04.27	36.43±01.70	60.50±01.10	32.37±00.74	44.20±02.87
TUEV	B-Acc	49.30±03.54	46.23±00.52	58.57±00.87	50.63±00.69	66.87±00.17	16.70±00.00	50.27±00.46
	F1/AUROC	70.10±05.93	73.37±00.48	74.93±01.62	80.87±00.92	81.83±00.82	44.10±00.00	74.33±00.42
	Kappa/AUCPR	52.80±09.26	55.60±00.85	58.83±02.39	69.43±01.55	69.73±01.24	00.07±00.09	55.90±00.67
TUAB	B-Acc	79.47±00.77	81.13±00.49	80.43±00.39	81.57±00.33	79.60±00.08	53.00±03.05	78.47±00.09
	F1/AUROC	89.43±01.05	90.27±00.40	89.17±00.91	89.17±00.33	87.43±00.73	58.90±11.39	87.73±00.09
	Kappa/AUCPR	89.77±01.01	90.53±00.45	89.70±00.36	89.23±00.12	88.00±00.36	53.13±09.31	86.33±00.40
HMC	B-Acc	60.47±03.28	66.73±00.31	67.70±00.41	58.80±00.45	68.77±00.21	20.00±00.00	70.17±00.29
	F1/AUROC	59.70±04.10	67.43±00.12	68.37±00.82	59.07±01.31	69.90±00.14	16.80±00.00	74.37±00.24
	Kappa/AUCPR	51.13±04.25	59.53±00.39	60.43±00.77	49.57±00.83	61.50±00.08	00.00±00.00	67.00±00.64
Siena	B-Acc	62.07±01.54	66.07±02.64	64.57±01.54	62.07±04.08	75.57±01.54	50.00±00.00	61.97±01.02
	F1/AUROC	92.90±03.43	79.37±04.79	89.27±03.11	93.10±00.73	92.20±01.48	42.53±32.12	74.07±01.19
	Kappa/AUCPR	99.87±00.05	99.30±00.14	99.80±00.08	99.90±00.00	99.87±00.05	66.23±46.83	99.27±00.05
TUSL	B-Acc	37.37±04.99	68.80±02.30	78.70±04.33	71.37±00.60	85.00±01.99	48.57±09.61	79.50±01.98
	F1/AUROC	21.53±09.24	64.50±03.88	71.30±05.30	68.90±02.98	79.80±03.47	43.10±14.54	80.53±02.10
	Kappa/AUCPR	03.50±04.74	50.50±03.64	60.67±06.76	53.10±02.98	71.60±03.82	23.30±15.21	70.27±03.35
Mimul-11	B-Acc	36.43±02.24	33.60±00.24	39.50±00.59	36.87±02.49	37.73±00.05	33.47±00.24	39.50±00.08
	F1/AUROC	43.37±03.78	41.70±00.29	46.57±00.97	42.60±03.52	46.70±00.16	39.80±01.84	47.80±00.82
	Kappa/AUCPR	07.00±04.96	01.07±00.90	11.90±00.83	07.33±05.15	09.37±00.42	00.33±00.47	12.47±00.68
Things EEG 2	B-Acc	50.00±00.00	50.00±00.00	50.13±00.05	50.00±00.00	53.53±01.01	50.10±00.14	52.37±00.31
	F1/AUROC	51.33±01.64	55.80±00.62	59.23±00.26	53.37±00.34	61.00±00.88	48.03±01.60	54.80±00.36
	Kappa/AUCPR	11.53±00.76	13.77±00.50	14.13±00.09	11.97±00.33	15.50±00.28	10.50±00.54	13.07±00.25
SEED-V	B-Acc	20.03±00.05	24.67±00.09	32.37±00.62	22.20±00.37	34.27±00.21	20.60±00.33	24.27±00.45
	F1/AUROC	09.43±00.53	22.70±01.00	30.83±00.86	16.50±01.45	34.20±01.22	09.47±02.38	22.67±01.76
	Kappa/AUCPR	00.07±00.09	06.70±00.37	16.30±00.65	03.53±00.61	18.23±00.34	00.70±00.37	05.50±00.37
ADFTD	B-Acc	33.90±00.43	46.23±00.45	45.97±01.10	44.17±01.25	45.83±00.69	33.30±00.00	39.73±00.34
	F1/AUROC	28.30±05.20	47.37±01.09	48.67±01.35	45.57±01.44	47.27±02.89	17.77±06.98	42.83±00.39
	Kappa/AUCPR	01.03±00.77	20.47±01.30	24.70±02.26	20.50±02.21	19.90±01.94	00.00±00.00	12.73±00.61
BCIC-2a	B-Acc	25.13±00.12	28.80±00.54	32.87±00.88	30.83±01.70	32.23±00.66	26.50±00.57	31.00±00.33
	F1/AUROC	13.83±04.34	20.50±01.73	28.13±02.88	24.23±03.35	27.97±01.48	18.77±02.02	30.30±00.33
	Kappa/AUCPR	00.13±00.12	05.10±00.70	10.50±01.21	07.80±02.30	09.63±00.88	01.97±00.78	08.00±00.49
SEED-VII	B-Acc	17.33±00.62	20.13±00.05	23.80±01.06	17.57±00.09	22.00±00.64	14.33±00.05	20.83±00.33
	F1/AUROC	09.47±00.25	17.80±00.49	21.13±01.96	10.73±01.09	18.53±00.73	04.43±00.54	20.50±01.27
	Kappa/AUCPR	03.80±00.37	07.50±00.08	11.37±01.27	04.37±00.17	08.57±00.78	00.03±00.05	08.03±00.34

Table 7. Performance comparison of 4 EEG-FMs on 13 BCI tasks under **full-parameter multi-task** fine-tuning with **attention pooling** classification head.

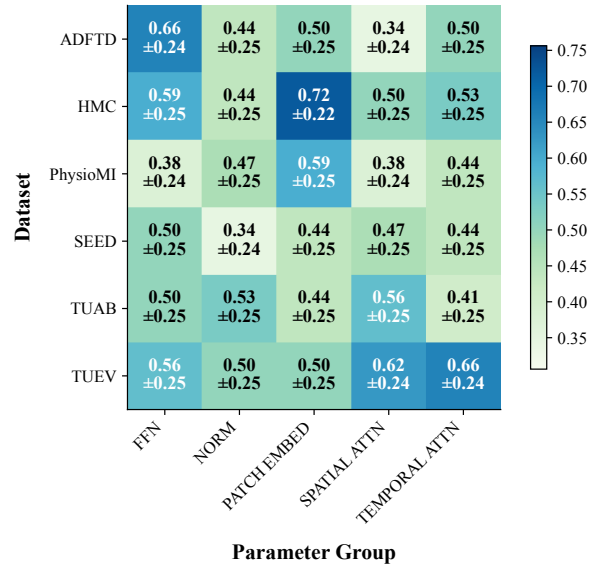
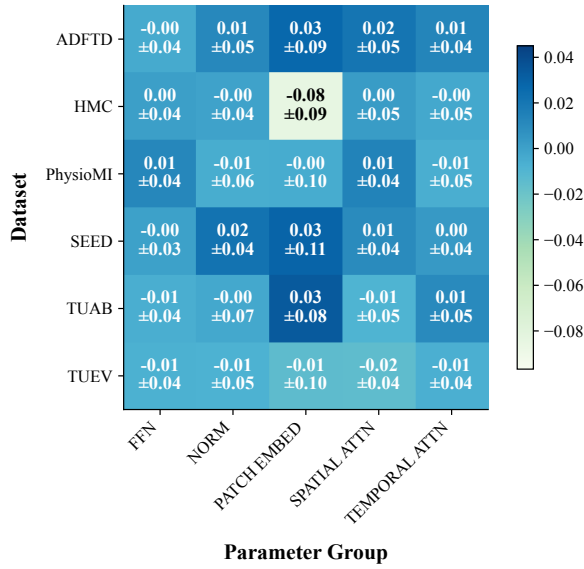
Dataset	Metrics	LaBraM	CBraMod	CSBrain	REVE
SEED	B-Acc	66.93±00.09	70.00±00.29	68.77±00.17	60.57±01.68
	F1/AUROC	66.43±00.09	69.40±00.50	67.93±00.48	60.50±01.61
	Kappa/AUCPR	50.53±00.17	55.13±00.49	53.30±00.22	40.97±02.54
PhysioMI	B-Acc	35.63±00.12	51.33±00.76	30.13±00.05	25.57±00.25
	F1/AUROC	34.50±00.22	51.27±00.73	29.37±00.49	19.93±05.70
	Kappa/AUCPR	14.23±00.12	35.10±01.00	06.83±00.05	00.73±00.34
Workload	B-Acc	76.00±00.28	73.63±01.84	71.27±00.75	71.27±03.87
	F1/AUROC	83.80±01.06	79.60±01.67	79.63±01.20	80.00±04.97
	Kappa/AUCPR	62.33±00.54	49.67±00.41	55.10±02.21	55.87±08.97
TUEV	B-Acc	81.00±01.53	66.67±00.46	73.90±01.31	59.20±00.78
	F1/AUROC	68.70±02.60	82.40±00.94	86.46±02.11	73.70±02.14
	Kappa/AUCPR	62.73±00.50	70.23±01.84	75.43±02.37	59.77±03.05
TUAB	B-Acc	80.47±00.52	82.07±00.53	78.23±00.12	80.53±00.39
	F1/AUROC	87.10±02.56	89.70±01.39	83.47±00.62	87.83±01.37
	Kappa/AUCPR	86.67±02.98	90.03±01.27	82.73±00.69	87.40±01.70
HMC	B-Acc	70.83±00.48	70.80±00.36	72.03±00.33	68.40±00.75
	F1/AUROC	71.00±00.67	71.30±00.86	74.60±00.29	69.73±01.19
	Kappa/AUCPR	63.20±00.78	63.93±00.90	66.17±00.40	61.30±01.10
Siena	B-Acc	74.03±01.89	81.87±00.47	72.07±02.92	62.07±01.16
	F1/AUROC	85.63±01.82	91.87±01.86	87.23±05.11	71.87±05.43
	Kappa/AUCPR	99.77±00.05	99.83±00.05	99.60±00.14	99.37±00.12
TUSL	B-Acc	69.17±00.21	83.53±01.04	68.77±00.90	72.97±03.94
	F1/AUROC	62.23±02.28	81.30±01.35	60.57±00.59	67.47±04.97
	Kappa/AUCPR	47.10±01.34	71.53±01.96	46.00±00.51	53.97±05.84
Mimul-11	B-Acc	38.50±01.02	41.87±00.78	42.10±00.51	44.03±00.50
	F1/AUROC	47.27±00.96	51.30±01.04	49.83±00.59	51.67±01.15
	Kappa/AUCPR	10.97±02.35	18.00±01.85	15.07±00.83	21.87±00.31
Things EEG 2	B-Acc	54.17±00.31	53.80±00.08	55.70±00.85	51.67±01.03
	F1/AUROC	56.47±00.12	59.97±00.91	62.93±00.81	58.80±02.34
	Kappa/AUCPR	15.30±00.00	16.60±00.37	19.60±00.75	14.67±01.39
SEED-V	B-Acc	54.17±00.31	37.90±00.22	38.90±00.45	20.73±00.33
	F1/AUROC	56.47±00.12	37.40±00.91	38.80±00.29	15.27±03.64
	Kappa/AUCPR	15.30±00.00	22.30±00.50	23.30±00.51	01.00±00.41
ADFTD	B-Acc	48.00±00.29	51.30±00.45	51.00±00.51	43.97±01.16
	F1/AUROC	51.33±00.68	52.13±01.44	53.90±00.51	45.10±00.24
	Kappa/AUCPR	25.17±01.11	27.37±01.30	28.77±00.77	18.80±00.29
BCIC-2a	B-Acc	33.23±00.26	36.67±01.11	33.70±00.28	31.80±00.29
	F1/AUROC	27.10±01.71	26.83±02.01	24.40±01.06	24.77±01.18
	Kappa/AUCPR	10.97±00.39	15.53±01.52	11.60±00.36	09.07±00.39

Table 8. Performance comparison of 4 EEG-FMs on 13 BCI tasks under **full-parameter multi-task** fine-tuning with **large compressing MLP** classification head.

Dataset	Metrics	LaBraM	CBraMod	CSBrain	REVE
SEED	B-Acc	71.34±00.33	74.70±00.64	72.20±00.45	64.46±02.11
	F1/AUROC	70.76±00.14	74.13±00.74	71.33±00.90	64.73±02.38
	Kappa/AUCPR	57.02±00.31	62.20±00.92	58.40±00.67	46.79±03.26
PhysioMI	B-Acc	57.52±00.27	61.73±00.25	55.60±00.16	48.26±01.24
	F1/AUROC	57.78±00.34	61.77±00.39	55.07±00.21	48.82±01.20
	Kappa/AUCPR	43.35±00.36	48.97±00.34	40.80±00.16	31.00±01.67
Workload	B-Acc	62.05±02.83	63.41±00.38	70.37±02.58	67.87±03.66
	F1/AUROC	74.82±01.89	71.00±00.17	81.73±00.95	81.40±02.20
	Kappa/AUCPR	52.48±04.74	46.43±01.47	63.00±03.82	59.77±07.16
TUEV	B-Acc	60.98±00.86	62.30±01.71	55.33±00.74	65.59±07.42
	F1/AUROC	77.86±00.53	79.63±02.07	76.33±00.74	75.94±00.12
	Kappa/AUCPR	63.13±01.28	66.17±03.60	60.70±01.28	62.16±00.56
TUAB	B-Acc	80.93±00.24	81.54±00.73	80.30±00.22	81.23±00.56
	F1/AUROC	87.90±00.96	87.93±01.27	85.87±00.90	88.27±00.40
	Kappa/AUCPR	87.35±00.88	86.61±01.45	84.00±00.50	85.93±00.90
HMC	B-Acc	70.45±01.19	72.10±00.33	70.27±00.57	68.16±00.62
	F1/AUROC	73.13±01.05	75.13±00.21	73.67±00.68	72.17±00.38
	Kappa/AUCPR	66.18±01.54	67.33±00.19	65.23±01.03	62.05±00.81
Siena	B-Acc	63.71±02.06	80.73±00.66	61.23±01.02	57.88±00.58
	F1/AUROC	84.13±02.78	84.70±05.26	89.97±00.69	63.20±01.57
	Kappa/AUCPR	99.67±00.06	99.63±00.12	99.73±00.05	99.18±00.04
TUSL	B-Acc	66.67±01.13	75.53±03.36	66.67±00.75	68.27±00.46
	F1/AUROC	59.00±01.36	73.37±04.73	53.83±02.99	66.73±01.97
	Kappa/AUCPR	41.60±01.87	60.27±06.65	40.60±02.20	50.03±01.48
Mimul-11	B-Acc	45.45±00.30	44.67±00.52	41.97±00.68	45.22±00.13
	F1/AUROC	52.59±00.38	51.73±01.01	49.90±01.70	53.73±00.65
	Kappa/AUCPR	21.38±00.63	20.40±01.42	16.07±00.57	21.53±01.16
Things EEG 2	B-Acc	52.46±00.60	52.87±00.09	51.10±00.71	54.40±00.41
	F1/AUROC	61.65±01.82	59.23±00.41	60.43±01.03	55.66±00.47
	Kappa/AUCPR	18.28±01.24	18.90±00.50	17.17±00.42	13.93±00.21
SEED-V	B-Acc	36.59±00.35	35.30±00.22	40.63±00.45	20.26±00.19
	F1/AUROC	36.58±00.31	36.00±00.42	41.27±00.25	09.71±00.52
	Kappa/AUCPR	20.66±00.48	19.43±00.40	25.87±00.29	00.40±00.31
ADFTD	B-Acc	47.97±00.20	53.27±01.72	49.90±00.42	39.97±00.05
	F1/AUROC	51.18±00.72	55.77±01.84	49.80±00.75	36.37±00.05
	Kappa/AUCPR	28.90±00.43	33.90±03.48	28.83±00.41	12.97±00.05
BCIC-2a	B-Acc	42.16±00.11	50.52±00.54	44.60±01.15	46.73±00.79
	F1/AUROC	41.25±00.17	49.15±00.72	41.07±02.04	45.33±01.26
	Kappa/AUCPR	22.88±00.14	34.03±00.71	26.13±01.56	35.56±00.73

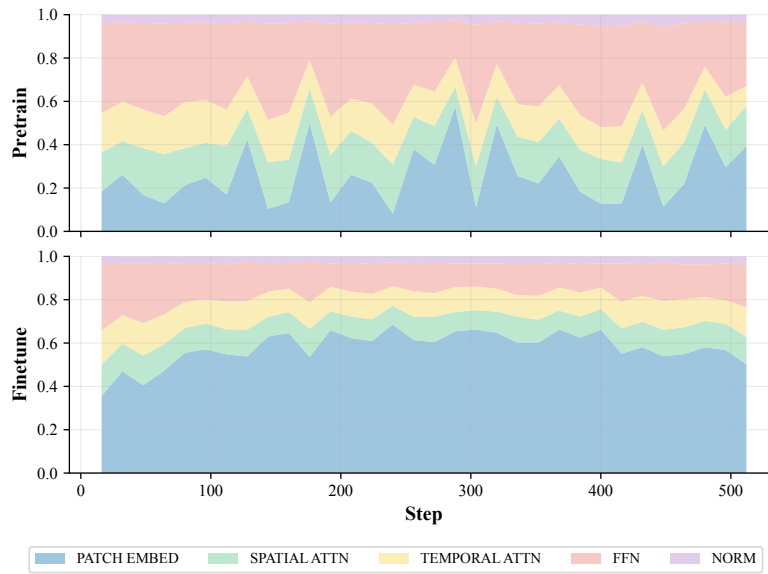
Table 9. Performance comparison of 2 foundation model for general time series on 14 BCI tasks under full-parameter multi-task fine-tuning with average pooling classification head.

Dataset	Metrics	Mantis			Moment		
		Full Param	Freeze	LoRA	Full Param	Freeze	LoRA
SEED	B-Acc	60.70±01.22	47.50±00.36	60.10±00.99	58.40±00.22	54.03±00.71	57.33±00.50
	F1/AUROC	60.97±00.86	43.97±01.17	59.27±01.58	56.50±00.80	52.60±01.27	54.70±01.45
	Kappa/AUCPR	41.17±01.92	21.37±00.54	40.33±01.44	37.80±00.37	31.20±01.04	36.13±00.71
PhysioMI	B-Acc	28.33±00.58	27.10±00.33	28.60±00.22	28.20±00.62	26.23±00.47	28.23±00.77
	F1/AUROC	22.20±01.23	19.27±02.31	24.37±00.56	23.80±02.08	18.03±02.29	22.67±02.69
	Kappa/AUCPR	04.43±00.74	02.80±00.41	04.77±00.26	04.23±00.82	01.60±00.64	04.30±01.02
Workload	B-Acc	63.33±02.68	62.73±01.05	63.93±01.60	62.43±02.09	50.00±00.00	53.70±05.09
	F1/AUROC	75.60±01.88	74.03±00.53	80.20±00.78	69.43±00.95	72.90±00.29	72.33±03.99
	Kappa/AUCPR	51.83±01.97	45.83±01.04	57.57±01.16	40.63±00.45	41.27±00.34	42.30±05.40
TUEV	B-Acc	67.00±00.70	52.97±00.54	54.93±00.09	64.03±01.28	42.43±00.70	59.87±00.09
	F1/AUROC	87.43±00.45	85.20±00.65	70.93±01.69	85.47±00.52	74.10±00.99	76.77±00.26
	Kappa/AUCPR	79.43±01.02	76.07±01.11	55.40±01.96	76.67±00.95	58.87±00.90	62.57±00.48
TUAB	B-Acc	79.67±00.26	75.97±00.12	76.93±00.19	77.87±00.24	74.30±00.28	77.80±00.36
	F1/AUROC	86.83±00.25	84.07±00.12	85.37±00.26	86.03±00.40	82.87±00.05	86.27±00.76
	Kappa/AUCPR	87.63±00.33	84.20±00.14	85.93±00.33	85.20±00.42	81.07±00.09	85.43±00.77
HMC	B-Acc	67.23±00.57	56.23±00.29	65.33±00.59	64.20±00.90	55.00±00.88	61.37±00.69
	F1/AUROC	71.10±00.54	60.17±00.65	69.23±00.81	68.00±00.92	58.23±00.82	64.87±00.38
	Kappa/AUCPR	63.03±00.41	49.47±00.76	61.00±01.19	59.67±01.11	48.13±01.08	55.33±00.56
Siena	B-Acc	72.47±02.68	53.70±00.00	61.23±01.67	66.67±02.91	52.40±00.99	64.93±02.67
	F1/AUROC	90.80±00.99	92.10±00.93	89.77±03.20	85.83±02.49	85.07±00.79	79.77±02.74
	Kappa/AUCPR	99.77±00.05	99.90±00.00	99.87±00.05	99.77±00.09	99.80±00.00	99.67±00.05
TUSL	B-Acc	78.00±01.18	65.57±03.14	71.37±02.32	69.63±02.59	40.87±00.38	59.50±02.65
	F1/AUROC	78.40±00.99	53.43±04.78	66.17±02.95	70.03±02.17	26.10±00.28	54.23±02.93
	Kappa/AUCPR	66.80±01.70	39.43±04.88	51.30±03.85	54.00±03.36	05.80±00.28	34.27±03.87
Mimul-11	B-Acc	42.63±00.87	40.33±00.47	41.00±00.08	40.57±00.83	34.37±00.50	40.43±00.91
	F1/AUROC	50.30±02.36	49.00±00.59	49.63±00.87	48.53±00.31	40.07±01.15	49.40±00.96
	Kappa/AUCPR	17.97±01.82	15.00±01.14	15.57±00.56	14.27±01.23	02.43±01.16	15.07±01.88
Things EEG 2	B-Acc	57.37±01.08	50.00±00.00	50.23±00.05	51.90±00.59	50.00±00.00	50.87±00.37
	F1/AUROC	67.10±00.57	60.63±00.68	59.63±01.05	63.00±00.37	56.47±00.98	61.20±02.20
	Kappa/AUCPR	27.07±01.23	15.90±00.29	15.40±00.50	19.83±00.54	13.37±00.65	18.60±01.28
SEED-V	B-Acc	24.57±00.80	21.10±00.22	23.70±00.33	22.10±00.36	20.00±00.00	21.57±00.52
	F1/AUROC	21.00±02.28	15.30±01.99	19.03±00.66	16.47±01.11	08.80±00.00	15.17±01.76
	Kappa/AUCPR	06.57±01.32	01.73±00.40	05.40±00.36	03.30±00.65	00.00±00.00	02.53±00.91
ADFTD	B-Acc	50.63±00.09	34.87±00.66	45.00±01.13	50.03±02.15	40.40±00.90	49.13±01.91
	F1/AUROC	48.70±00.36	30.97±03.54	44.77±01.32	48.93±01.89	38.53±01.92	46.87±02.13
	Kappa/AUCPR	30.77±00.12	02.83±01.18	21.10±01.84	29.60±03.72	13.63±01.72	28.23±03.24
BCIC-2a	B-Acc	34.43±00.74	31.93±00.45	31.63±00.77	32.53±00.83	27.97±02.50	29.07±00.74
	F1/AUROC	28.40±01.39	27.03±00.60	24.90±02.01	25.27±01.43	15.37±03.28	18.70±01.53
	Kappa/AUCPR	12.57±00.97	09.30±00.57	08.87±01.03	10.10±01.06	03.97±03.35	05.43±00.95
SEED-VII	B-Acc	18.97±00.87	18.00±00.22	19.03±00.26	19.73±00.37	17.80±00.08	20.67±01.43
	F1/AUROC	16.17±01.01	15.73±00.69	17.27±01.06	17.87±00.42	14.60±00.14	17.73±02.00
	Kappa/AUCPR	06.23±01.14	04.83±00.31	06.30±00.33	07.43±00.53	04.73±00.12	08.70±02.00



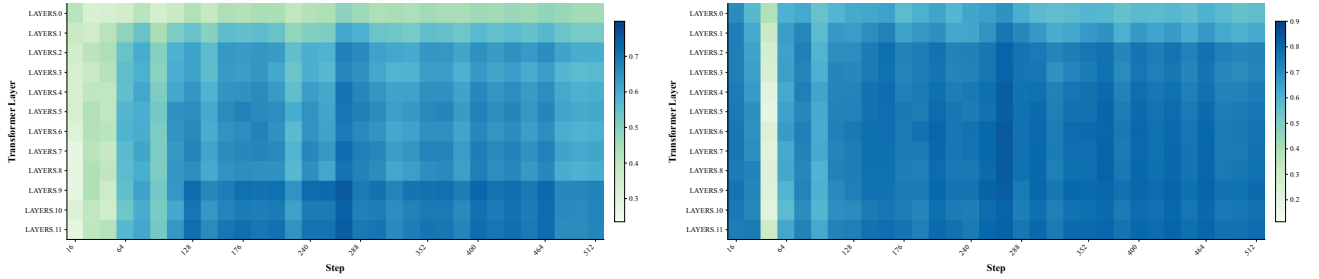
(a) Cosine similarity across datasets and parameter groups.

(b) Gradient conflict frequency.



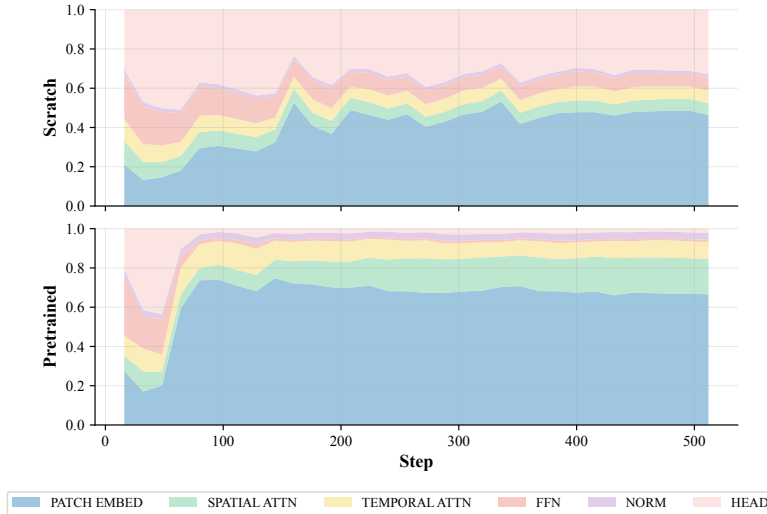
(c) Relative gradient norm intensity across modules.

Figure 18. Gradient alignment between pre-training and downstream tasks for CBraMod.



(a) CKA analysis for representations across backbone layers.

(b) RSA analysis for representations across backbone layers.



(c) Relative gradient norm intensity across modules.

Figure 19. Evolution of optimization dynamics during fine-tuning between from scratch and from pretrained checkpoint for CBraMod.

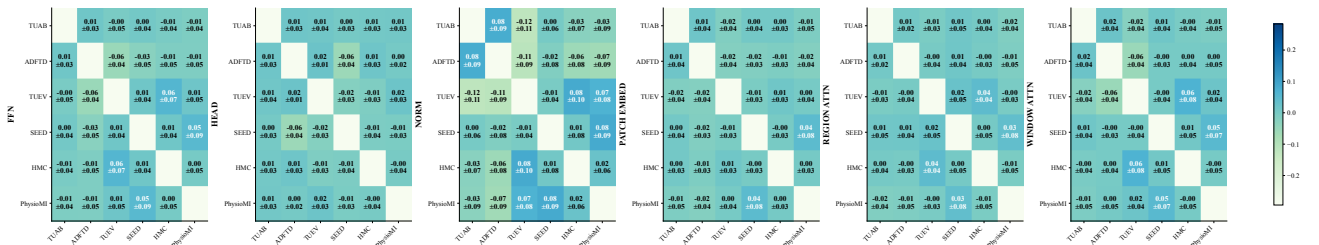


Figure 20. Cross-task gradient correlation analysis for CSBrain.

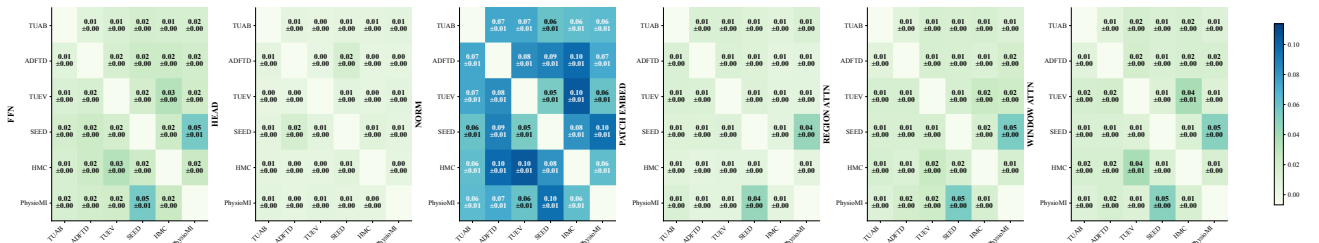


Figure 21. Cross-task subspace affinity analysis for CSBrain.

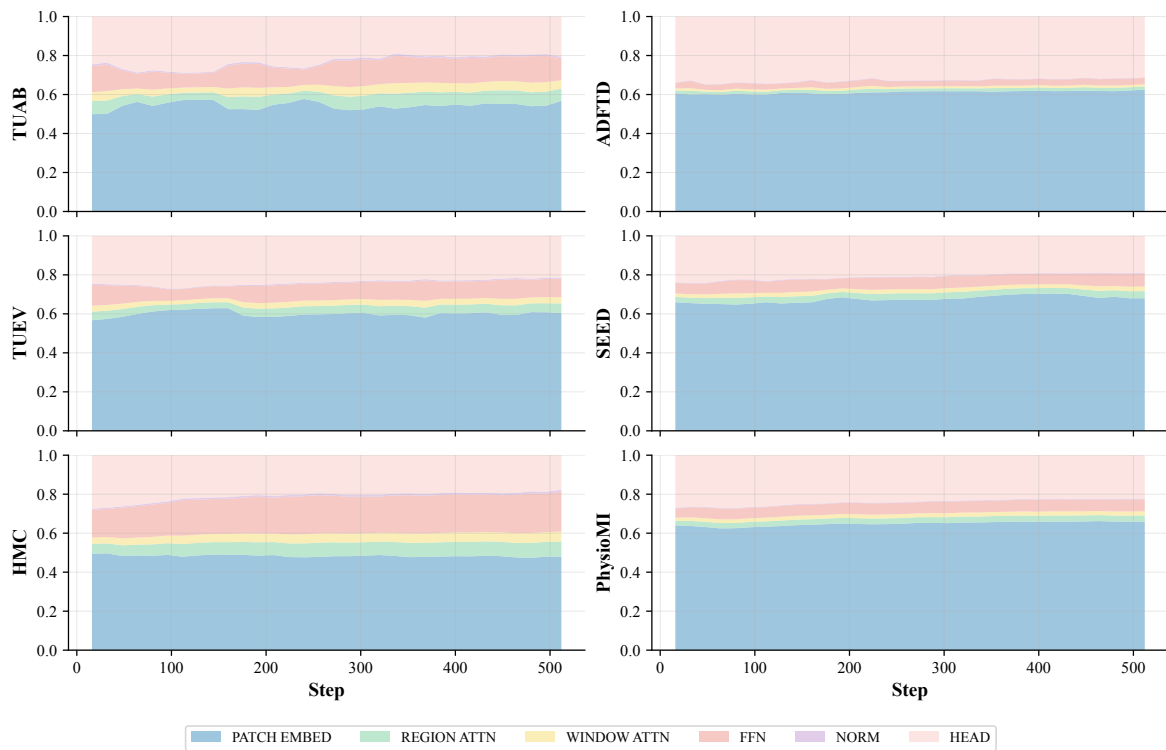
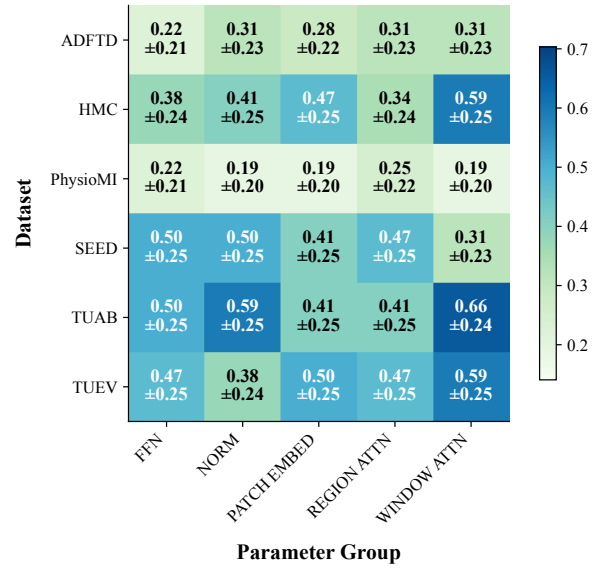
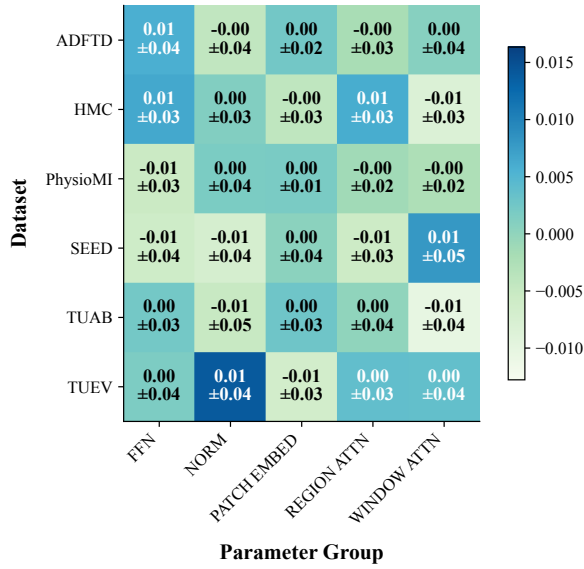
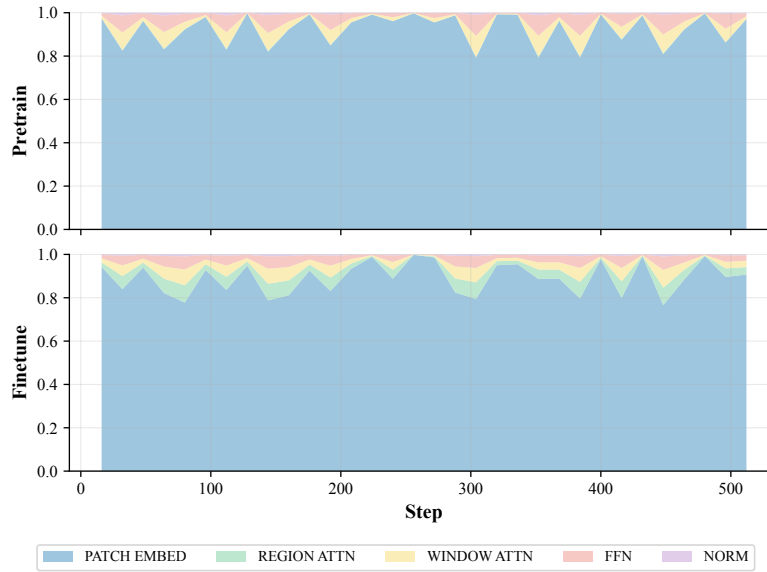


Figure 22. Cross-task evolution dynamics analysis for CSBrain.



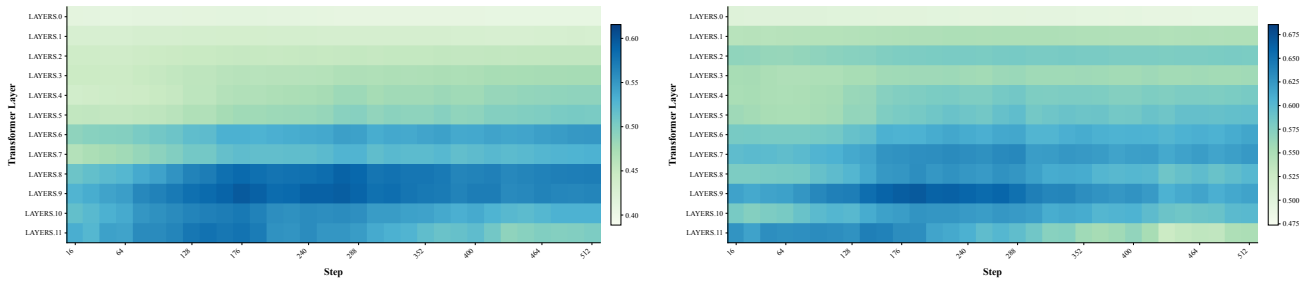
(a) Cosine similarity across datasets and parameter groups.

(b) Gradient conflict frequency.



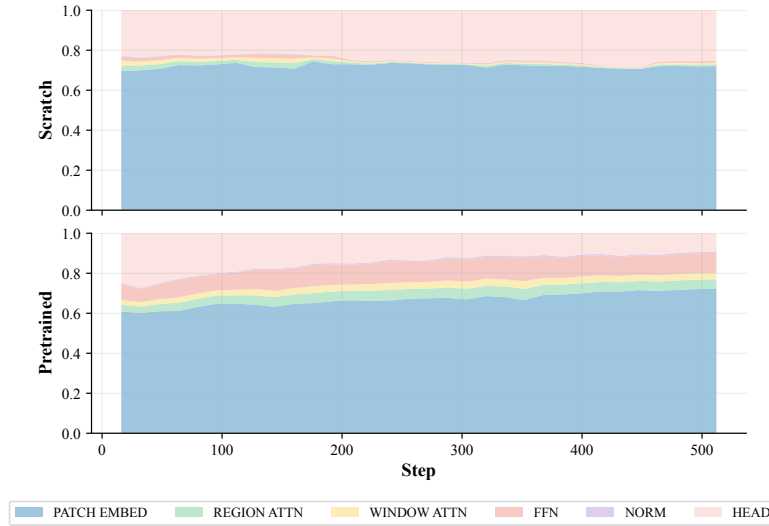
(c) Relative gradient norm intensity across modules.

Figure 23. Gradient alignment between pre-training and downstream tasks for CSBrain.



(a) CKA for representations across backbone layers

(b) RSA for representations across backbone layers



(c) Relative gradient norm intensity across modules.

Figure 24. Evolution of optimization dynamics during fine-tuning between from scratch and from pretrained checkpoint for CSBrain.

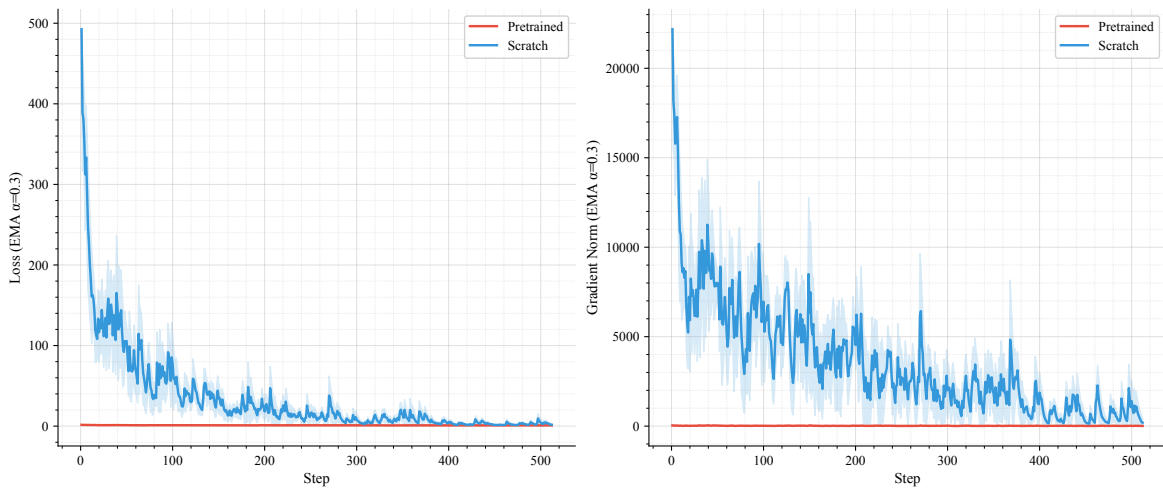


Figure 25. Training loss and gradient norm during fine-tuning between from scratch and from pretrained checkpoint for CSBrain.

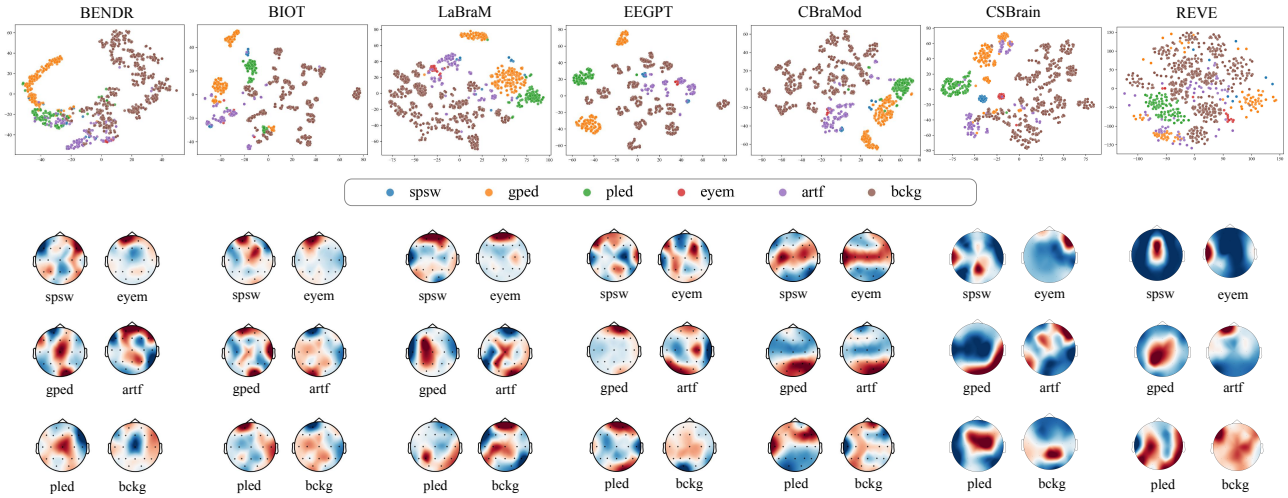


Figure 26. Visualization of models prediction results on TUEV.

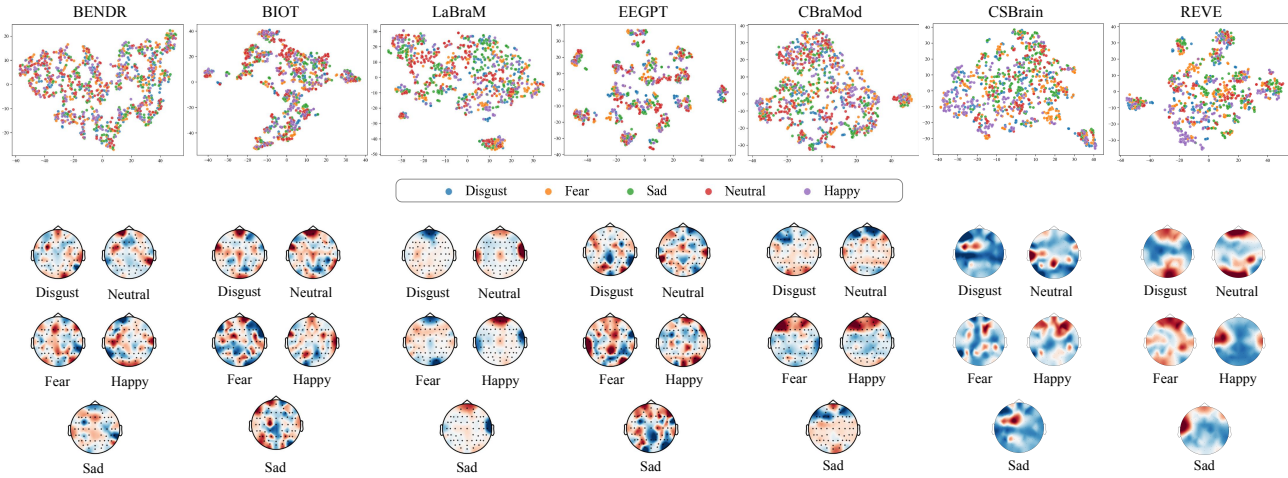


Figure 27. Visualization of models prediction results on SEED-V.

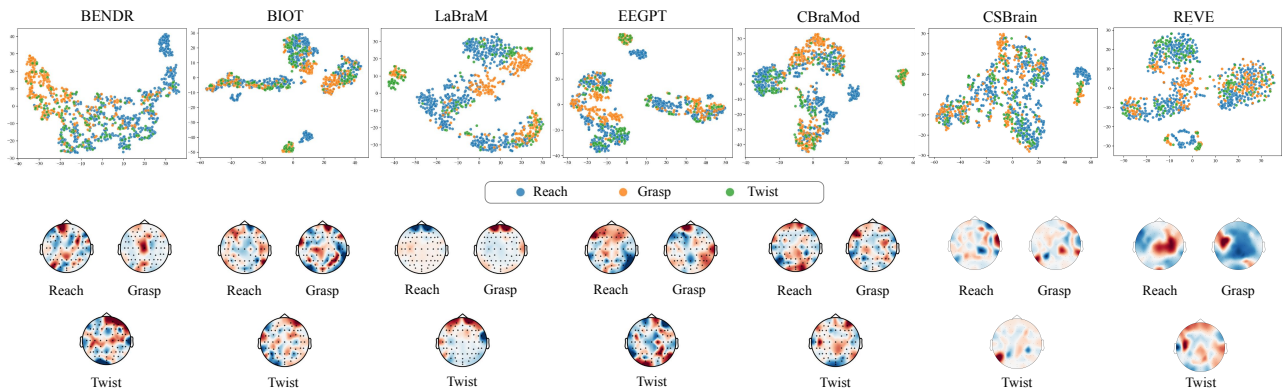


Figure 28. Visualization of models prediction results on Mimul-11.

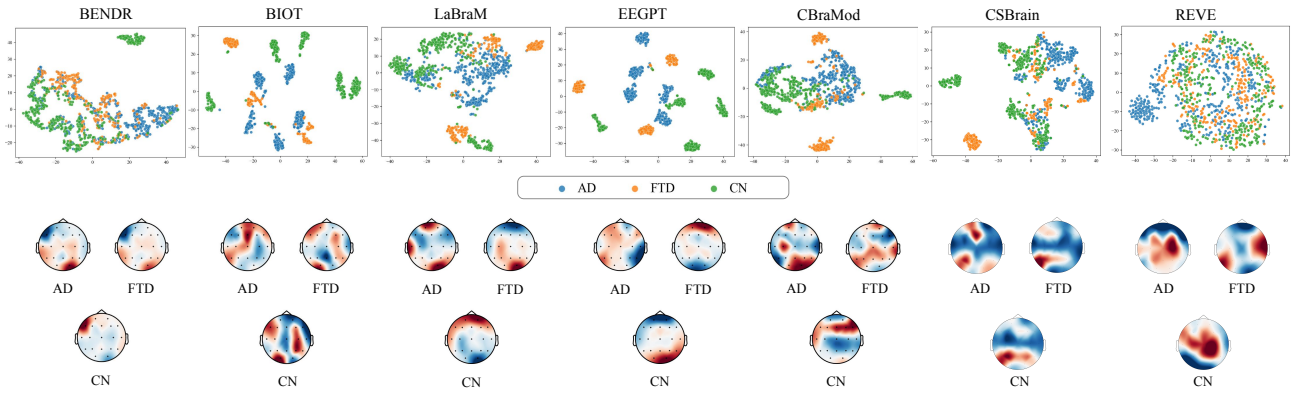


Figure 29. Visualization of models prediction results on ADFTD.

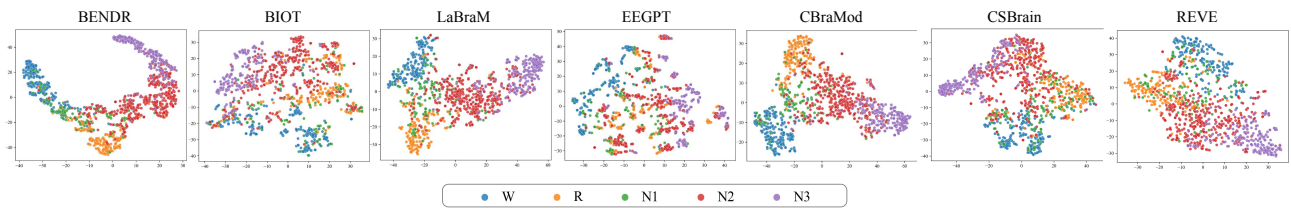


Figure 30. Visualization of models prediction results on HMC.